Forward/pA Physics at RHIC-II Whitepaper

January 26, 2006

Convenors:
Carl Gagliardi
Mike Leitch
and Kirill Tuchin

1 EXECUTIVE SUMMARY 1

2 GLUON SATURATION AND SHADOWING 4

3 FORWARD HADRON SUPPRESSION IN D+AU COLLISIONS 15

4 HEAVY QUARKS AT FORWARD RAPIDITY 16

5 FORWARD TAGGED PROCESSES 26
5.1 TAGGED DRELL-YAN PROCESSES 26
5.2 TAGGED FORWARD PROTONS 27

6 ANTI-QUARK DISTRIBUTION IN NUCLEI AT SMALL X 27

7 ULTRA-PERIPHERAL PROCESSES 28

8 DOUBLE PARTON CORRELATIONS 30

9 COMPARISON OF RHIC-II AND LHC HEAVY-ION PROGRAMS 31

10 RHIC DETECTOR UPGRADES 31
10.1 PHENIX UPGRADES 31
10.1.1 MUON TRIGGER UPGRADE 31
10.1.2 SILICON VERTEX DETECTOR 33
10.1.3 NOSE CONE CALORIMETER 36
10.2 STAR UPGRADES 37
10.2.1 FORWARD SILICON TRACKER 38
10.2.2 FORWARD CALORIMETER? 38

11 APPENDIX: RATES FOR FORWARD AND P(D)+A PROCESSES 39

12 APPENDIX: TOP-DOWN PHYSICS CHARTS 40

List of Figures

Figure 1 - Kinematic space of QCD. Arrow points out to the novel high parton density regime of cold nuclear matter, the Color Glass Condensate, which arises at small x and/or large nuclei. 5
Figure 2 - Kinematic regions of high energy QCD. 8
Figure 3 - Gluon production amplitude in p(d,γ^*) A collisions in terms of the fan-diagrams. 9
Figure 4 - Prediction of CGC for the total charged particle multiplicity in dAu collisions. 10
Figure 5 - Calculations based on CGC versus RHIC experimental data. One can see transition from the quasiclassical regime at midrapidity to the quantum evolution regime at forward rapidities. 10
Figure 6 - (see caption to Figure 5). 11
Figure 7 - Depletion of two particle correlations due to gluon saturation. 11
Figure 8 - Enhancement of Cronin effect with rapidity as predicted by the rescattering models. 12
Figure 9 - Rapidity asymmetry ratio. 13
Figure 10 - A parameterization of gluon shadowing. 13
Figure 11 – Preliminary measurement by PHENIX of prompt muons (from charm and beauty decays) in the foward rapidity or small-x region (red) and in the backward rapdity region (blue). 17
Figure 12 - STAR $D \rightarrow K\pi$ signal in d+Au collisions at 200 GeV/c. 18
Figure 13 - J/ψ and ψ' suppression from E866/NuSea' compared to calculations from R. Vogt showing the many ingredients invoked to explain the dramatic x_F dependence of the observed suppression. 20
Figure 14 - J/ψ suppression at √S=200 GeV from PHENIX vs rapdity compared to model calculations from R. Vogt for EKS shadowing and different $c\bar{c}$ absorption cross sections in the final state. 21
Figure 15 – Preliminary results for the nuclear modification factor in AuAu and CuCu collisions from PHENIX vs centrality for forward and central rapidity compared to CNM calculations consistent with those shown in the previous figure (Figure 14). 22
Figure 16 - Comparision of J/ψ nuclear suppression for three different beam energies showing the lack of scaling vs x_2 and approximate scaling seen vs x_F. 23
Figure 17 - Ratio of central to peripheral yields per binary collision for d+Au collisions comparison between J/ψ's (PHENIX) and light hadrons from Brahms and PHENIX. A similar pattern is seen with a small enhancement at negative rapidity (Au direction) and suppression at postitive rapidity (d direction and small-x shadowing region). 24
Figure 18 - Preliminary PHENIX ϒ results at forward and backward rapidity (red) from 200 GeV p+p collisions compared to measurements at other energies vs energy. 25
Figure 19 – Simulation of the neutron-tagged Drell-Yan process where the muons are detected in the PHENIX muon arms and the neutron in a small-angle calorimetet (e.g. the PHENIX ZDC). 26

Figure 20 – J/ψs produced in ultraperipheral Au+Au collisions at RHIC from PHENIX. 30
Figure 21 - PHENIX Muon Trigger upgrade (one arm shown) with its RPC planes shown in black, existing muon tracking detectors in red. The primary interaction region is at the right-center of the figure. 33
Figure 22 - PHENIX Silicon Vertex Detector Upgrade including the forward vertex detector (FVTX) and central barrel vertex detector (VTX). 34
Figure 23 - The reconstructed Z-vertex distribution for J/ψ from B decays (black line) and for prompt J/ψ (red line). Note that the J/ψ yield has been scaled down by a factor of 100. The relative yield of J/ψ from B decays versus prompt J/ψ is estimated to be about 1%. 35
Figure 24 - Mass spectra for the J/ψ and ψ', showing the substantial improvement in separation expected with a vertex detector (yellow, 100 MeV resolution) compared to that without a vertex detector (black, 150 MeV resolution). The number of J/ψ and ψ' in this plot represents our expectation for a ~25 pb^{-1} p+p run. 36
Figure 25 - PHENIX Nose Cone Calorimeter (NCC) upgrade (purple). 37
Figure 26 - STAR Forward Silicon Tracker upgrade. 38
Figure 27 - STAR ? upgrade. 38
Figure 28 - Top-down physics chart for gluon saturation and shadowing in nuclei..... 40
Figure 29 - Top-down physics chart for anti-quark distributions in the nucleon sea (Jen-Chieh Peng). 41

List of Tables

Table 1 - Rates for the PHENIX forward vertex detector (FVTX) in one week of running. Integrated luminosities are 33 pb^{-1} for p+p, 62 nb^{-1} for d+Au, and 2.5 nb^{-1} for Au+Au (RHIC-II) and 9.9 pb^{-1} for p+p, 2.8 nb^{-1} for d+Au and 0.33 nb^{-1} for Au+Au (RHIC-I, 2008). The semileptonic decay rates are before application of a vertex cut. 19

Table 2 - Beam energies, E_{beam}, Lorentz factors, γ_L, photon cutoff energy in the center of mass frame, $k_{\max}$, and in the nuclear rest frame, $E_{\max}$, and equivalent nucleon-nucleon center of mass energy, $\sqrt{S_{\max}}$, for *AA* collisions at RHIC. 28

1 Executive Summary

The suppression of various processes in p(d)+A collisions at forward rapidity is usually thought to be caused by shadowing or saturation of the gluons in nuclei for the small momentum fraction (x) region. Shadowing is a depletion of the structure functions in the small-x region thought to result from coherence effects on the process of interest that depend on the momentum of the incoming parton or by saturation of the population of the small-x gluons[1] that may cause two-to-one gluon diagrams to depopulate the smallest x gluons and possibly enhance those at moderate x values (anti-shadowing). The shadowing of quark distributions is well established from deep inelastic scattering measurements, but that for the gluons largely comes from only the Q^2 evolution of these same measurements and so is poorly known experimentally. Theoretical models for gluon shadowing are numerous and differ both in their underlying physics and, by large factors, in the predicted amount of gluon shadowing[2,3,4]. Underlying physics ideas include the coherence effects and gluon saturation mentioned already, but also may involve energy conservation effects (Sudakov suppression), energy loss in the initial state of the incoming gluons or partons, or mass renormalization effects. These fundamental physics ideas abound and overall leave a rather unsettled picture for which processes are truly important and control the fundamental dynamics of partons (gluons) in nuclei. In addition they are not well constrained by present experimental measurements and there is a strong need for more precise measurements that will isolate and constrain these fundamental physic issues. Since these intrinsic properties of the gluons in nuclei provide the initial state for nucleus-nucleus collisions, it is also critical to understand them in order to obtain a clean baseline for the study of hot-dense matter effects in nucleus-nucleus collisions, e.g. in the study of the Quark Gluon Plasma.

It has also been observed that the production of many types of particles at forward rapidity appear to follow a universal suppression pattern with even hadrons at different energies following this trend (in the rapidity gap from the kinematical limit), often called limiting fragmentation[5], although it is not clear what physics might be the source of such a phenomena.

At RHIC our measurements explore the onset of this shadowing or saturation, while at the LHC most measurements will lie deep in the saturation region. We believe that studying the onset will be key to understanding the saturation phenomena and that studies at RHIC and RHIC-II will be complementary and supporting for those at the LHC. At the LHC the p+A program is still considered an upgrade especially in terms of running the accelerator for these collisions and we are not likely to see such collisions until 2010 at the earliest. In addition, it is likely to be quite difficult to run p+A collisions a the LHC given that only approximately one month a year will be devoted to “heavy ion” running and that the p+A running (along with all the heavy-ion running) will have to come out of this time.

Some of the most compelling physics questions are:

- Shadowing or saturation of the gluon densities at small-x and pinning down the underlying physics that controls these phenomena with precise measurements of a wide range of observables.
- Power corrections in open charm production (Vitev and Qiu)[6].
- Study of limiting fragmentation[5], Sudakov suppression[7] and other phenomena that may also be key ideas in the behavior of particle production in p(d)+A collisions at forward rapidity.
- Parton recombination pictures that also provide an explanation for the forward-rapidity suppression[8].
- Quantifying the energy loss and multiple scattering of partons in cold nuclear matter.
- Disentangling the complicated physics puzzle for J/ψ suppression in cold nuclear matter using accurate and robust measurements of both open- and closed-charm (J/ψ and ψ'); and similarly for beauty production and ϒ's.
- Searching for mono-jets as a signature of gluon saturation[9].
- Double-parton correlations from 4-jet yields[10] which can only be done with p+A collisions.
- Processes tagged with forward neutrons or protons to isolate the structure of the nucleon's meson cloud or to explore gluon-rich states via Pomeron exchange
- Ultra-peripheral collisions which provide a theoretically clean probe, e.g. of the gluon distributions in nuclei via J/ψ production[11].

The most compelling measurements that will need RHIC-II luminosities are:

- Heavy-quark measurements are rare processes and require the highest luminosities to obtain the accuracy and reach needed to isolate the fundamental physics questions of interest. In particular J/ψ and ϒ measurements and also measurement of b-mesons via $B \rightarrow J/\psi\ X$ and d-mesons via $D \rightarrow K\pi$
- Ultra-peripheral collision measurements, which without much higher luminosities than presently available, will remain very low statistics measurements and of little value for quantitative studies.
- Forward nucleon-tagged measurements which are inherently low-rate and need the highest luminosities possible. [are these even possible at RHIC-II?]
- Double parton correlations via 4-jet events which clearly require the highest luminosites. [what are the rates?]

[Most compelling physics that can benefit from RHIC-II luminosities compared to RHIC-I with and w/o detector upgrades; and comparison to LHC of these processes.]

A number of critical detector upgrades to the large RHIC detectors will also be necessary in order to effectively pull off these measurements and provide the wide range of accuate and robust measurements necessary to pin down the fundamental physics questions. These include:

- The PHENIX Silicon Vertex detector, with the VTX at central rapidity ($|y|<1$) and the FVTX at forward and backward rapidity ($1<|y|<2.2$), will enable precise measurements of open-charm and beauty and improve signal-to-noise and resolution for numerous other measurements.
- The PHENIX Nose Cone Calorimeter (NCC) which will provide calorimetry in the forward and backward rapidity regions and allow measurements in the $1<|y|<3$ rapidity region of direct photons to probe the gluons and $\chi_C \rightarrow J/\psi\ \gamma$ to provide the χ_C part of the J/ψ puzzle.
- The PHENIX Muon Trigger upgrade which will allow triggering at RHIC-II luminosities on very high momentum muons - in particular for those coming form the decay of W mesons, but also providing fast triggering momentum information that will allow the level-1 triggers necessary to capture many of the processes discussed here at RHIC-II luminosoties.
- The STAR Forward Meson Spectrometer (FMS)
- The STAR Forward Tracker (with GEM's)
- Upgrades of the data-acquisition and triggering systems for both detectors to allow capture of all the processes of interest in the highest luminosity RHIC-II running.
- Additional additions to our detector arsenal, e.g. to allow tagging with very forward protons using Roman pots.

The convenors of this working group are Carl Gagliardi, Mike Leitch and Kirill Tuchin. A number of other people have been involved in the meetings and discussions, these include: Tony Baltz, Les Bland, Ramiro Debbe, Tony Frawley, Wlodek Guryn, Yuri Kovchegov, Pat McGaughey, Jen-Chieh Peng, Peter Steinberg, and Ramona Vogt. Because of the highly parallel nature of the various RHIC-II Science Physics working groups, it was difficult to involve many members of the community who had involvement in the other groups; and also for those involved in our group, especially the convenors to fully participate in the discussion of the other groups. We also note that many of the physics topics that are important here were also discussed in other groups, most notably the heavy-quark group which has a large overlap with ours.

In this document we include 1) this executive summary, 2) followed by several sections discussing the most compelling physics areas in more detail, then next 3) a discussion of the upgrades for the RHIC detectors and their role in achieving the physics, 4) a comparision with the LHC program, and then two appendices giving a) selected rate estimates for RHIC-II measurements, and b) the "top-down" physics charts that were formulated by our working group.

2 Gluon Saturation and Shadowing

Perturbation theory plays the key role in establishing Quantum Chromodynamics as the theory of strong interactions. It has been very successful in describing particle production in processes with high momentum transfer. It relies on the collinear factorization theorems which allow separation of the short distance processes calculable using the standard methods of perturbation theory and the non-perturbative long distance processes. The basic idea is that the short and long distance processes become incoherent when the momentum transfer becomes sufficiently large. The long distances processes can be parameterized by the universal distribution functions which depend on the momentum scale Q^2 and Bjorken variable x. Once a distribution is measured as a function of x at a given value Q_0^2 its evolution at higher values of Q^2 is determined by the DGLAP evolution equations.

Despite its tremendous success at short distances, perturbation theory describes only a small part of the full QCD. In fact, it does not allow us study the beautiful non-linear structure of QCD. This structure reveals itself at long distances where the coupling becomes strong not allowing for systematic theoretical treatment. However, this structure can be accessed also at small x where the fields become strong while the coupling is weak. Alternatively, strong fields at weak coupling can be created in processes with large nuclei.
The first signatures of the new regime of QCD came from the Deep Inelastic Scattering experiment at HERA. It has been observed that the gluon and sea quark distributions grow very fast with decreasing x. This fast growth can be understood in pQCD as driven by radiation of gluons with small Bjorken x via DGLAP evolution equations. Radiated gluons form a *high parton density system* which cannot be described using the collinear factorization scheme due to strong coherence effects. There is a more fundamental reason to abandon the collinear factorization at small x and/or large nuclei: the fast growth of parton distribution functions cannot continue forever since it would lead to growth of hadronic cross sections at a rate which would violate unitarity. This necessitates extension of the pQCD framework to include the nonlinear effects of parton recombination and saturation.

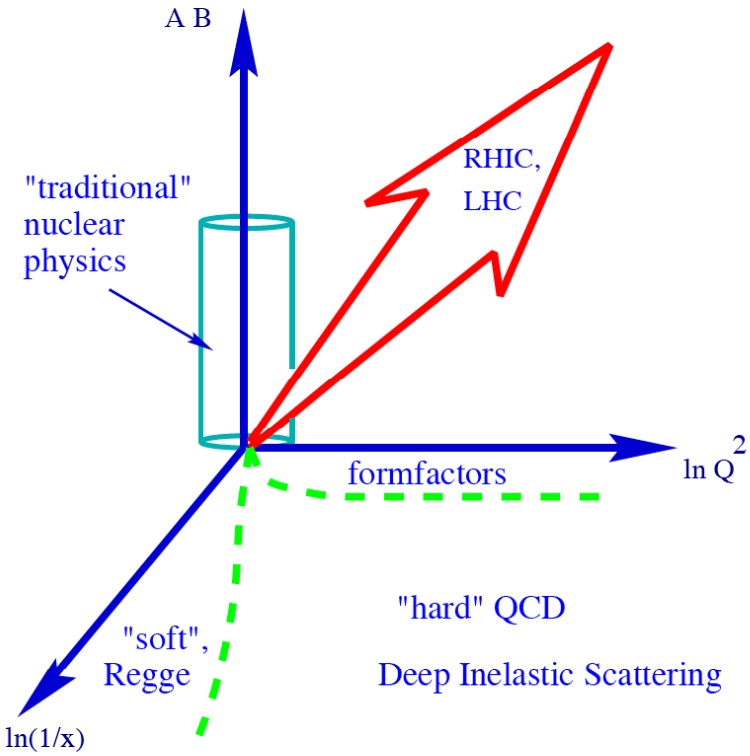

Figure 1 - Kinematic space of QCD. Arrow points out to the novel high parton density regime of cold nuclear matter, the Color Glass Condensate, which arises at small x and/or large nuclei.

Quasiclassial approximation

Color Glass Condensate formalism is the natural generalization of pQCD in order to make it applicable to dense partonic systems [12]. It provides a consistent way of systematic treatment of high energy parton evolution and the nuclear coherence effects. Coherence effects start to play a significant role in a scattering process at small x. When the parton coherence length l_c in the projectile proton (deuteron) becomes larger than the size of the target nucleus R

$$l_c = \frac{1}{2m_N x} > R \qquad \textbf{Equation 1}$$

the projectile interacts coherently with all nucleons along its path through the nucleus. Here m_N is a nucleon mass. In this situation the total cross section is given by the sum over all possible interactions of p(d) with any number of nucleons. Such interactions are suppressed in the weak coupling regime. However, if the nucleus is sufficiently heavy so that $\alpha_s^2 A^{1/3} \sim 1$, then these interactions are large. They can be resumed if we note that the parton distribution in the projectile does not evolve during the interaction with the nucleus if $l_c >> R$. In particular, it is convenient to consider a projectile as a collection of color dipoles with certain transverse sizes r_t. The size of each such dipole is fixed during the interaction. The

forward scattering amplitude of a (q anti-q) dipole on a nucleus is then given by the Glauber-Mueller formula

$$N(Y, r_\perp, b_\perp) = 1 - \exp\left(-r_\perp^{\,2} Q_s^{\,2}/4\right) \quad \textbf{Equation 2}$$

where Y=ln(1/x) and we introduced the following notation

$$Q_s^2 = \frac{\alpha_s \pi^2}{2N_c} \rho T(b_\perp) x G_N(x, 1/r_\perp^2) \quad \textbf{Equation 3}$$

with T(b) being the nuclear profile function, and xG_N the gluon distribution in a nucleon taken at some fixed value x. The momentum scale Q_s is called the saturation scale since the scattering amplitude reaches its unitarity limit (saturates) at N=1for dipoles $r_t>1/Q_s$. The ratio of $N(x,r_t,b)$ and the first term in its expansion at small α_s is always smaller than 1. Therefore, Equation 2 effectively sums up "shadowing corrections" due to multiple rescattering of the projectile in the nucleus. Smallness of the coupling is ensured by the existence of the hard scale Q_s. Phenomenological analysis of the particle production at RHIC gives Q_s=1-2GeV which is large enough to keep the coupling small $\alpha_s(Q_s)<<1$. The total p(d)A cross section can be calculated by convoluting Equation 2 with the parton distributions in a proton (deuteron).

Equation 2 makes it possible to include the coherence effects in p(d)A collisions at not very small x. Indeed, it is derived neglecting possible emission of a gluons and quark–antiquark pairs in the high energy projectile. It is this emission which leads to fast increase of the gluon and sea quark distribution functions observed in γ^*p collisions at HERA. Parametrically, each emitted gluon gives contribution of the order of $\alpha_s \ln(1/x)$ to the scattering amplitude and can be neglected if $x>\exp(-\alpha_s)$. Therefore, one usually refers to Equation 2 as the quasiclassical approximation to the scattering amplitude valid for the following values of x:

$$e^{-\alpha_s} < x < \frac{1}{2m_N R} \quad \textbf{Equation 4}$$

Similarly, we can consider gluon or light quark production in p(d)A collisions. Due to large coherence length of a low x gluon, its radiation in a projectile wave function occurs way before (or after) the interaction with the target. The radiation kernel is well-known in pQCD and is given by (in the coordinate space)

$$\frac{\alpha_s C_F}{\pi} \frac{r_{01}^2}{r_{20}^2 r_{21}^2} \quad \textbf{Equation 5}$$

where 0,1 are the coordinates of the initial quark and antiquark and 2 is the coordinate of the emitted gluon in the transverse plane. Scattering of each dipole in a system of quark, antiquark, and gluon is given by Equation 2. The cross section for the gluon production in p(d)A collisions is

$$\frac{d\sigma}{d^2kdy} = \frac{1}{\pi}\int d^2bd^2rd^2z\frac{1}{(2\pi)^2}\frac{\alpha_s C_F}{\pi}\frac{r\cdot z}{r^2z^2}e^{-ik_t\cdot(r-z)}\left[N_G(0,r,b)+N_G(0,z,b)-N_G(0,r-z,b)\right]$$

Equation 6

where N_G is the gluon dipole scattering amplitude taken at some initial rapidity Y=0. This formula can be cast in a more traditional form using the unintegrated gluon distribution $\phi(x,q_t)$ function

$$\phi(x,q_t) = \frac{C_F}{\alpha_s(2\pi)^3}\int d^2bd^2ze^{-iq_t\cdot z}\nabla_z^2 N_G(y=-\ln x,z,b)$$ **Equation 7**

The inclusive cross section takes then the k_T-factorized form

$$\frac{d\sigma}{d^2kdy} = \frac{2\alpha_s}{C_F k^2}\int d^2q\phi_p(y=0,q)\phi_A(y=0,k-q)$$ **Equation 8**

An important feature of the quasiclassical approximation is that the transverse momentum of the projectile dipoles gets redistributed in course of multiple rescattering in the nucleus. This property follows from the following sum rule

$$\int d^2kk^2\frac{d\sigma^{pA}}{d^2kdy} = A\int d^2kk^2\frac{d\sigma^{pp}}{d^2kdy}$$ **Equation 9**

Multiple rescattering tends to increase the transverse momentum of the projectile. Since the typical transverse momentum transfer is Q_s^2 , production of gluons with momentum $k\sim Q_s$ is enhanced in pA collisions as compared to pp ones. Equation 9 implies then suppression of soft gluon production in pA collisions. In experimental data this redistribution of particle momentum is known as the Cronin effect. Therefore, appearance of the Cronin enhancement is a necessary feature of the quasiclassical regime of CGC.

High energy quantum evolution

As the energy of the collision increases, the multiple gluon radiation becomes parametrically large. A gluon radiated with the light-cone momentum fraction $x<\exp(-\alpha_s)$ contributes at the order $\alpha_s y\sim 1$ to the scattering amplitude. Radiation of a gluon at rapidity $Y+\Delta Y$ leads to change in the amplitude $\Delta N(Y,r_t,b)$. There are two physical processes contributing to increase of the amplitude: multiplication of gluons proportional to $\alpha_s N$ and recombination proportional to $-\alpha_s N^2$. The Balitsky-Kovchegov evolution equation takes both processes into account

$$\frac{\partial N(Y,r_t)}{\partial Y} = \frac{\alpha_s C_F}{\pi^2}\int dx_2 \frac{x_{01}^2}{x_{12}^2 x_{20}^2}\left[N(Y,x_{02}) + N(Y,x_{12}) - N(Y,x_{01}) - N(Y,x_{02})N(Y,x_{12})\right]$$

Equation 10

This equation has been derived in the large Nc approximation and neglecting target correlations. Together with the initial condition Equation 2 it allows to calculate the forward amplitude of the dipole-nucleus scattering at high energies.

As the result of the evolution of the amplitude N at high energies the average gluon momentum acquires its energy and rapidity dependence

$$Q_s^2 = \Lambda^2 A^{1/3}(s/s_0)^{\lambda/2} e^{\lambda y}$$ **Equation 11**

The line $Q=Q_s(s,y)$ divides the kinematic plane (Q^2,y) into two regions. The saturation region $Q<<Q_s(s,y)$ in which the scattering amplitude is close to unity and the dilute region $Q>>Q_s(s,y)$ in which the effect of multiple rescattering described by the nonlinear term in the Equation 10 is small. Solution to Equation 10 exhibits a remarkable property of 'geometric scaling': in the saturation regime the amplitude N depends on x and Q only via one dimensionless parameter Q/Q_s in agreement with the low x experimental data at HERA.

.

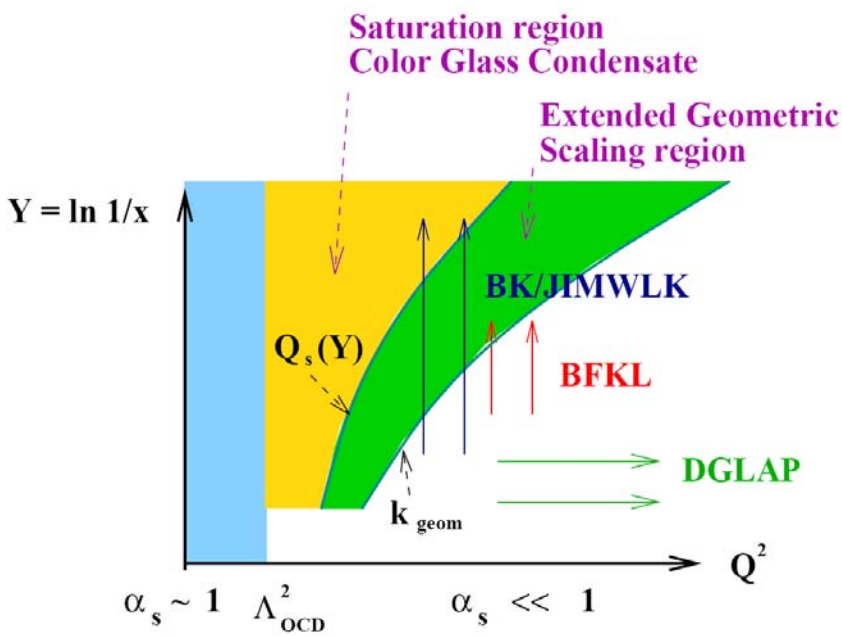

Figure 2 - Kinematic regions of high energy QCD.

Condition N<<1 is necessary for the applicability of the collinear factorization theorems. However, it is not sufficient since the low x evolution in the vicinity of the saturation

boundary is still driven by the BFKL dynamics. Transition from BFKL to DGLAP dynamics happens when $\alpha_s y \sim \alpha_s \ln(Q_s/ Q_{s0}) < \alpha_s \ln(Q/Q_s)$, i.e. $Q > Q_s^2/ Q_{s0}$. Since the amplitude N geometrically scales along $Q=Q_s(s,y)$ and the LO BFKL equation is conformally invariant, N also geometrically scales in the wide kinematic region $Q<k_{geom} = Q_s^2/ Q_{s0}$. A more accurate estimation yields for the boundary of the 'extended geometric region'

$$k_{geom} = Q_s(Y)\left(\frac{Q_s(Y)}{Q_{s0}}\right)^{0.34} \quad \textbf{Equation 12}$$

The kinematic plane of high energy QCD is shown in Figure 2.

Inclusive gluon production cross section can be written in a k_T-factorized form similar to Equation 8

$$\frac{d\sigma}{d^2kdy} = \frac{2\alpha_s}{C_F k^2}\int d^2q\phi_p(Y-y,q)\phi_A(y,k-q) \quad \textbf{Equation 13}$$

where ϕ now depend on energy and rapidity. The typical gluon production amplitude (squared) is shown in Figure 3.

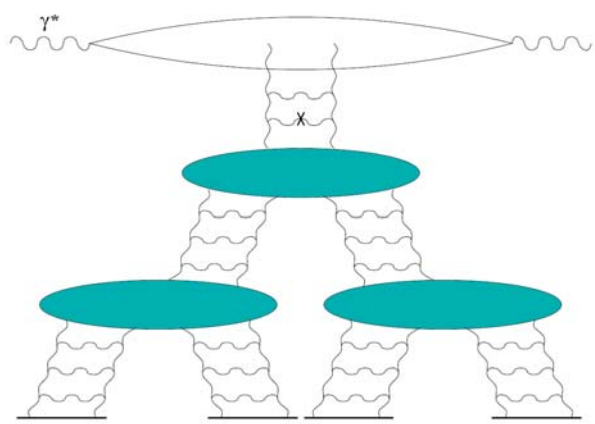

Figure 3 - Gluon production amplitude in p(d,γ^*) A collisions in terms of the fan-diagrams.

While in the quasiclassical approximation (not very small x, see Equation 4) the inclusive gluon cross section satisfies the sum rule Equation 9, it breaks down at low x when the evolution effects become important. It opens a possibility of suppression of nuclear modification factor R_{pA} for gluon production in the extended geometric scaling region. In the saturation region the main physics mechanism of R_{pA} suppression is multiple rescattering of a gluon in the nucleus. In the extended geometric scaling region, higher twist terms $(Q_s/k)^{2n}$ are small. However, the anomalous dimension of the unintegrated gluon distribution function of nucleus near the saturation boundary is about ½. In the same kinematic region, gluon distribution in proton has the anomalous dimension about 1. This reflects itself in the peculiar dependence of the nuclear modification factor on A: $R_{pA} \sim A^{-1/6}$.

A detailed analysis yields

$$R_{pA} \approx A^{-0.124} < 1 \quad \textbf{Equation 14}$$

Suppression of the nuclear modification factor Equation 14 due to dependence of the anomalous dimension of the gluon distribution function on energy and rapidity can be refereed to as the 'leading twist shadowing'.

One can think of the Color Glass Condensate approach as of a theory of leading and higher twist shadowing based on pQCD (in the sense of weak coupling). Phenomenological approaches based on CGC are successful in describing the low x DIS data. In particular, we should mention prediction of the geometric scaling, description of diffractive processes and fit of the structure functions. In dA collisions the experimental data on hadron production are in agreement with the CGC predictions, see Figures 4,5,6

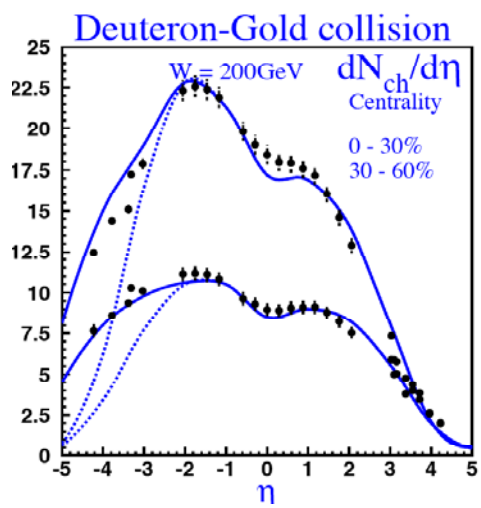

Figure 4 - Prediction of CGC for the total charged particle multiplicity in dAu collisions.

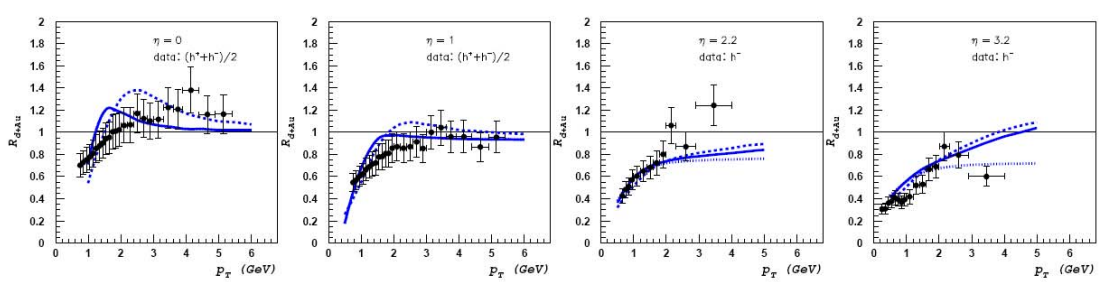

Figure 5 - Calculations based on CGC versus RHIC experimental data**.** One can see transition from the quasiclassical regime at midrapidity to the quantum evolution regime at forward rapidities.

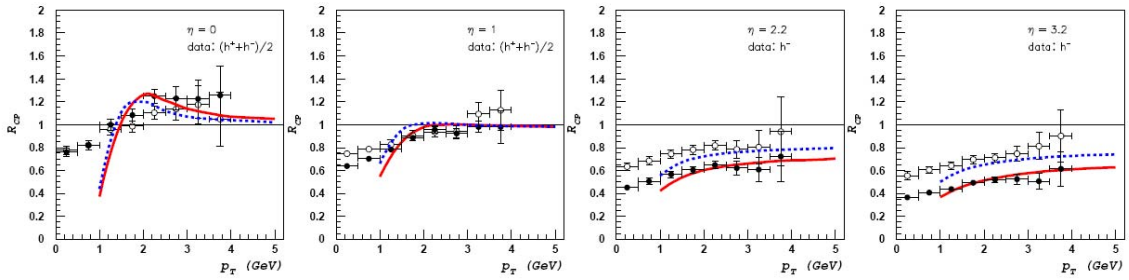

Figure 6 - (see caption to Figure 5)

Equation 8 describes a single gluon production. This process is kinematically permitted due to transverse momentum dependence of the unintegrated gluon distributions ϕ. For gluons with transverse momentum much larger then the typical transverse momentum transfer Q_s Equation 9 reduces to the familiar collinear factorized result. However, bulk of gluons are produced as monojets. This implies depletion of the back-to-back correlations which are inherent to the QCD processes at very high momentum. This depletion is enhanced at higher energies/forward rapidities as shown in Figure 7.

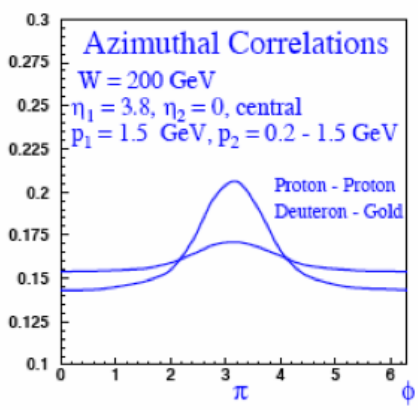

Figure 7 - Depletion of two particle correlations due to gluon saturation.

Other inclusive channels such as heavy quark, quarkonium and dilepton production can be calculated in the same framework provided that the coherence length of the considered probe is much larger than the nucleus size. Heavy quark production by a classical color fields is of special theoretical interest. Large mass m of a quark justifies application of perturbation theory regardless of the value of Q_s . Thus we can study the onset of the classical regime of QCD as Q_s approaches m as well as production of heavy quarks in saturated medium Q_s >>m. Production pattern of light and heavy quarks in strong color fields is the same. Therefore one expects similar suppression effect on heavy quarks at Q_s>>m.

Alternative approaches

As has been already discussed, there is a certain kinematic region, Equation 4, where small x evolution effects are small and multiple rescattering of a projectile in a nucleus accounts for the observed particle spectra. One can try to extend this approach to higher energies/rapidities. Momentum transfer in each individual projectile-nucleon scattering is proportional to the parton density which is increasing function of 1/x. Therefore, the average momentum gained by the rescattering parton increases with energy/rapidity implying enhancement of the Cronin effect: both the position and the height of the maximum increase as shown in Figure 8.[13]

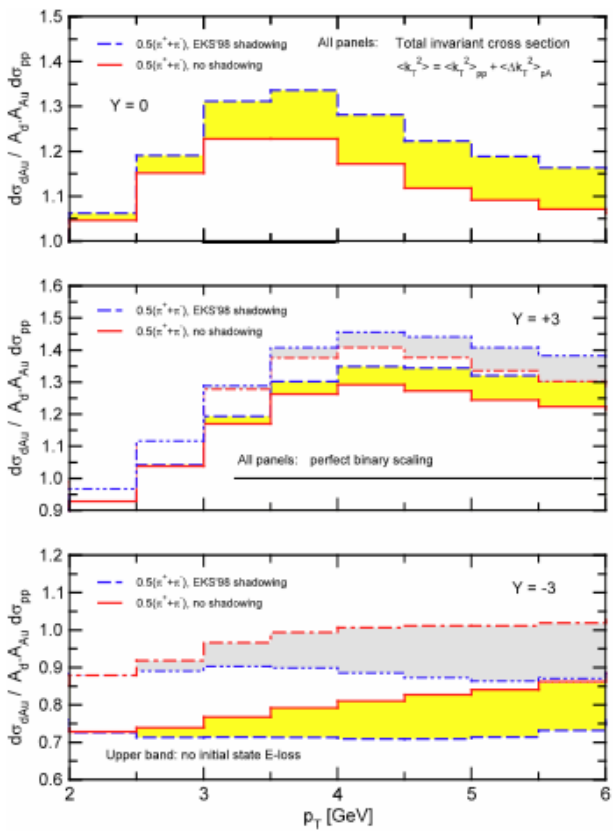

Figure 8 - Enhancement of Cronin effect with rapidity as predicted by the rescattering models.

This model is suitable for description of the Cronin effect at midrapidity. However, its failure at forward rapidities implies that there must be an additional suppression in the parton distribution function itself.

The forward-backward rapidity asymmetries of hadron production in dAu collisions shown in Figure 9 (three lower curves) is another prediction of a rescattering model improved by inclusion of a nuclear shadowing effect[14]. Again, it seems that the data favors the CGC shadowing mechanism (upper two curves).

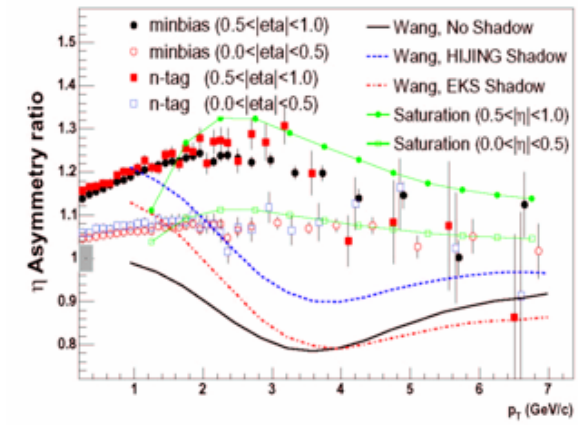

Figure 9 - Rapidity asymmetry ratio.

It has been suggested by Kopeliovich at. al.[15] that the observed suppression of the nuclear modification factor at midrapidity is a consequence of the rapid decrease of the phase space available for gluon production at $x_F \rightarrow 1$. This fragmentation effect is energy independent. On the contrary, the effect of gluon saturation increases with energy which provides a clear experimental handle to distinguish between the two physics mechanisms.

Another set of models uses traditional collinear factorization approach to particle production in pA collisions. The shadowing effect is then parameterized by the A-dependent parton distribution functions [16], as shown in Figure 10.

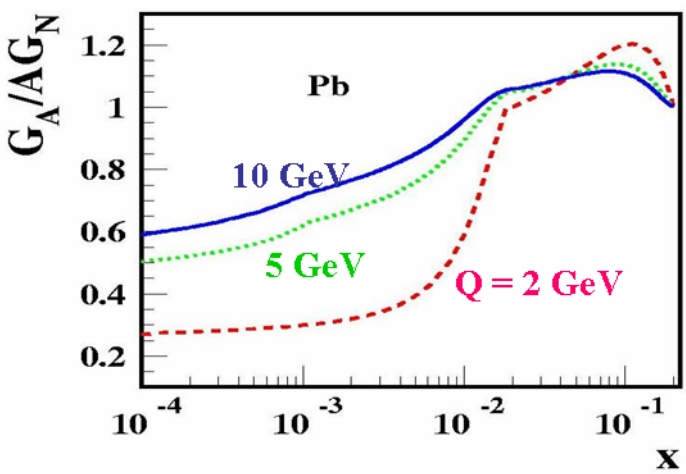

Figure 10 - A parameterization of gluon shadowing.

However, it was argued in [17] that none of existing shadowing parameterizations can describe the magnitude of experimentally observed suppression.

In the case of ptoton-heavy nucleus collisions one can extend the pQCD analysis of particle production in the framework of the collinear factorization by summing up all higher twist terms of the type $(\xi^2 A^{1/3}/Q^2)^N$ where $\xi^2 \sim \alpha_s$ is a non-perturbative matrix element proportional to xG[18]. The resumation parameter in this approach is $\alpha_s A^{1/3} \sim 1$ (compared to $\alpha_s^2 A^{1/3} \sim 1$ in CGC). The result can be written in a collinear factorized form with the shift of Bjorken variable $x \rightarrow x(1+\xi^2(A^{1/3}-1)/Q^2)$ which leads to a net suppression of the cross sections. Approach of Ref.7 fills the gap between the leading twist collinear factorization picture and the CGC.

It was suggested in [19] that parton recombination may play an important role in particle production at RHIC. In particular, parton recombination in the final state may be responsible for the suppression of the nuclear modification factor at forward rapidity.
This idea deserves further investigation.

Future experimental studies

The RHIC experimental data from dA and AA collisions seems to favor the discovery of a new form of cold nuclear matter. RHICII offers a unique possibility to confirm this discovery and study properties of the new form of nuclear matter. The following experimental studies are of great importance:

- Particle production at high transverse momentum. The higher transverse momentum, the better we know how to take into account the non-perturbative processes such as parton fragmentation.
- Two particle correlations. Depletion of particle correlations is a very important signal of CGC, see Figure 6.
- Charm and charmonium production at forward rapidities. The effect of quantum evolution in open charm production may be seen already at rapidity 2-3 at RHIC.
- Electromagnetic signatures: photon and dilepton production offer a more precise tools to study the quantitative aspects of QCD matter at high energies.

3 Forward Hadron Suppression in d+Au Collisions

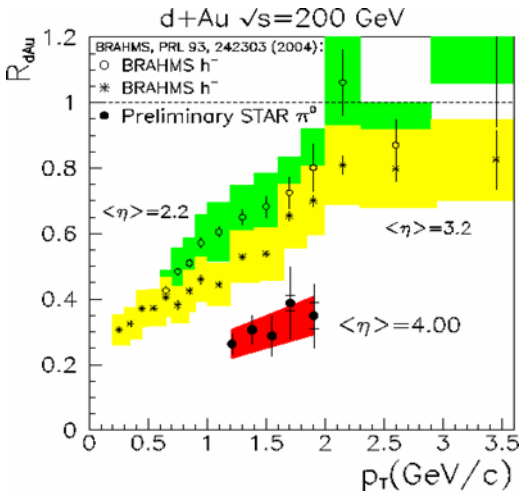

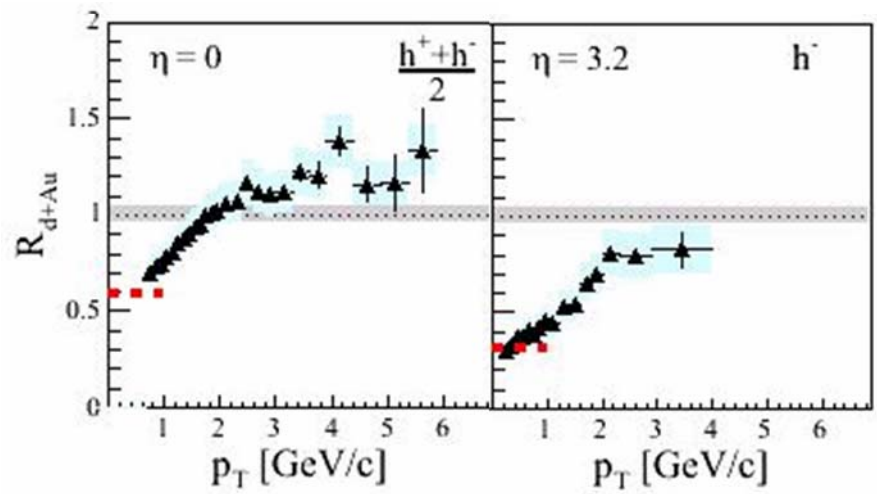

4 Heavy Quarks at Forward Rapidity

Heavy quarks provide an important tool for accessing gluon distributions since they are produced primarily through diagrams involving gluons, mainly gluon fusion. In p(d)+A collisions they give a window into the gluon distribution in "cold nuclear matter" (CNM) and thus can provide a measure of the shadowing or saturation of the gluon distributions in nuclei.

Heavy quarks are created early and therefore sample the entire evolution of the collision. In heavy-ion collisions their momentum distributions can then be used to measure their energy loss in the high-density matter created in those collisions, while in p(d)+A collisions we can set a baseline on this energy loss for CNM. In addition, the multiple-scattering of the gluon in the initial state – sometimes called the Cronin effect, can be seen in the broadening of the p_T distributions of the heavy quark or of their bound states.

Another group in this study, the Heavy-Quark RHIC-II Science working group, has concentrated on the complete heavy-quark picture for all kinds of collisions, so here we will focus mainly on their study in p(d)+A collisions.

Open charm and beauty, presently, are accessed primarily through their decays to leptons (electrons or muons). These measurement rely on a statistical subtraction of background sources, i.e. for electrons the other sources of electrons including π^0's, photon conversions, etc are subtracted in a so-called "cocktail" analysis; while for muons the copious backgrounds from light hadrons decays and hadrons that "punch through" the absorbers of the muon identifier are substracted. This results in large systematics due to the knowledge of the subtracted backgrounds. A preliminary measurement from PHENIX with muons in the forward and backward rapidity regions is shown in Figure 11, where a suppression for the forward rapidity is seen. Also shown, in Figure 12 is the $D \rightarrow K\pi$ signal seen in the STAR detector.

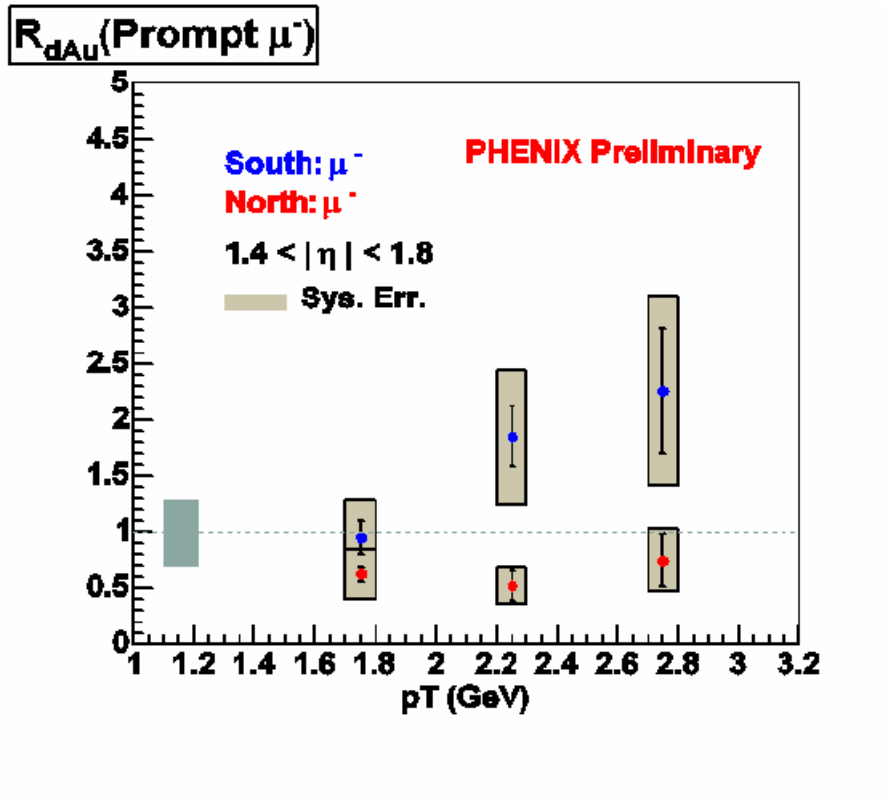

Figure 11 – Preliminary measurement by PHENIX[20] of prompt muons (from charm and beauty decays) in the foward rapidity or small-x region (red) and in the backward rapdity region (blue).

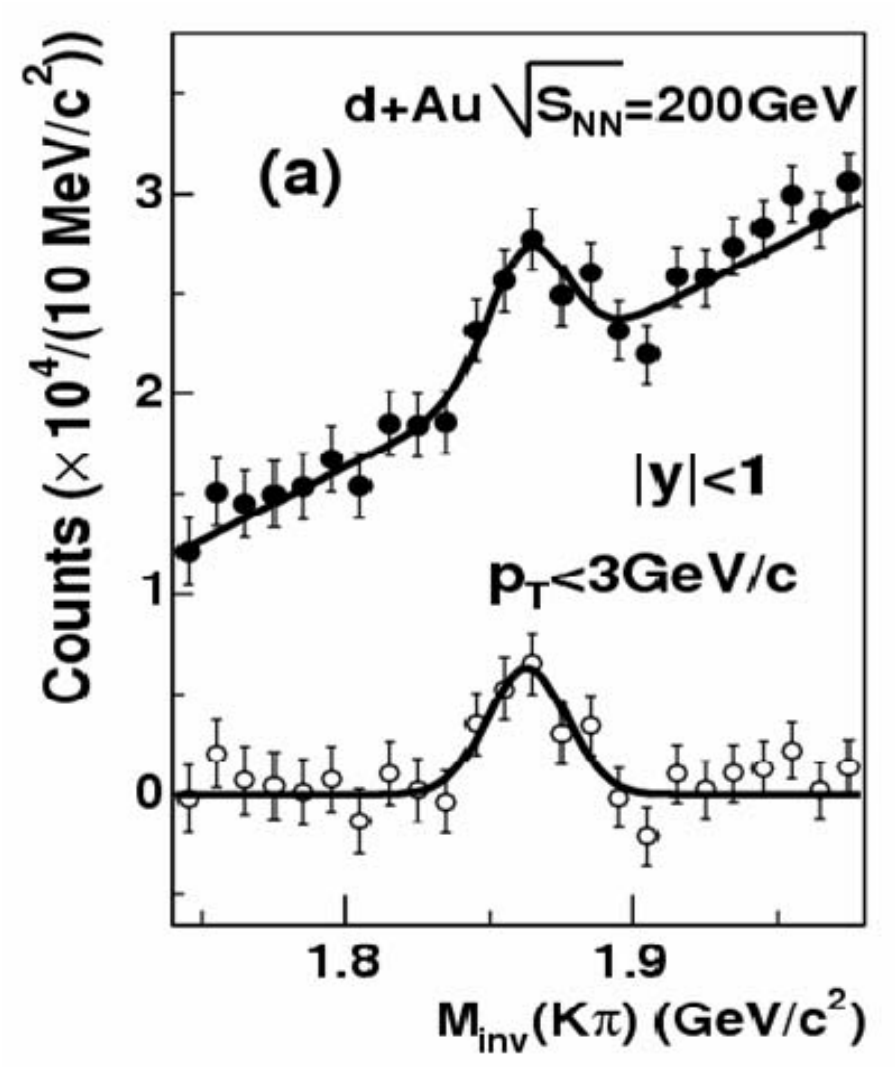

Figure 12 - STAR $D \rightarrow K\pi$ signal[21] in d+Au collisions at 200 GeV/c.

Future detector upgrades to allow explicit observation on an event-by-event basis of the small but finite decay distance of the charm or beauty mesons are planned, but to reach large momenta and adequately separate charm and beauty in these spectra will require higher luminosity runs. In particular, explicit measurements of the process B $\rightarrow$ J/ψ X will be important in measuring the B cross section independently so that the then known B cross section can be used to separate out the beauty and charm contribution to the single lepton spectra. As can be seen in Table 1, large luminosities will be required to get substantial numbers of B $\rightarrow$ J/ψ X events, and to extend the single-lepton measurements to larger p_T values.

Table 1 - Rates for the PHENIX forward vertex detector (FVTX) in one week of running. Integrated luminosities are 33 pb^{-1} for p+p, 62 nb^{-1} for d+Au, and 2.5 nb^{-1} for Au+Au (RHIC-II) and 9.9 pb^{-1} for p+p, 2.8 nb^{-1} for d+Au and 0.33 nb^{-1} for Au+Au (RHIC-I, 2008). The semileptonic decay rates are before application of a vertex cut.

	p+p counts/week		**d+Au counts/week**		**Au+Au counts/week**	
Observable	**RHIC-I**	**RHIC-II**	**RHIC-I**	**RHIC-II**	**RHIC-I**	**RHIC-II**
$D \to \mu X$	84M	21M	2.7M	60M	24M	180M
$D \to \mu X$, $4<p_T<5$ GeV	3.1k	10k	400	8.8k	3.5k	27k
$B \to \mu X$	260k	880k	33k	740k	300k	2.3M
$B \to \mu X$, $4<p_T<5$ GeV	2.7k	9.1k	340	7.6k	3.1k	24k
$B \to J/\Psi X \to \mu^+\mu^-$	200	650	25	550	220	1.7k

The suppression in p(d)+A collisions remains a complicated physics puzzle with a number of different effects that may contribute to the complex pattern observed in fixed target measurements and at RHIC. The x_F dependence of the suppression for J/ψ and ψ' from E866/NuSea[22,23] is shown in Figure 13 along with model calculations from R. Vogt[24]. In this model a large number of physics ingredients are included in order to explain the data. Alternative explanations include models[7] where Sudakov suppression, an energy conservation effect, operates to force an increasing suppression as one approaches $x_F = 1$.

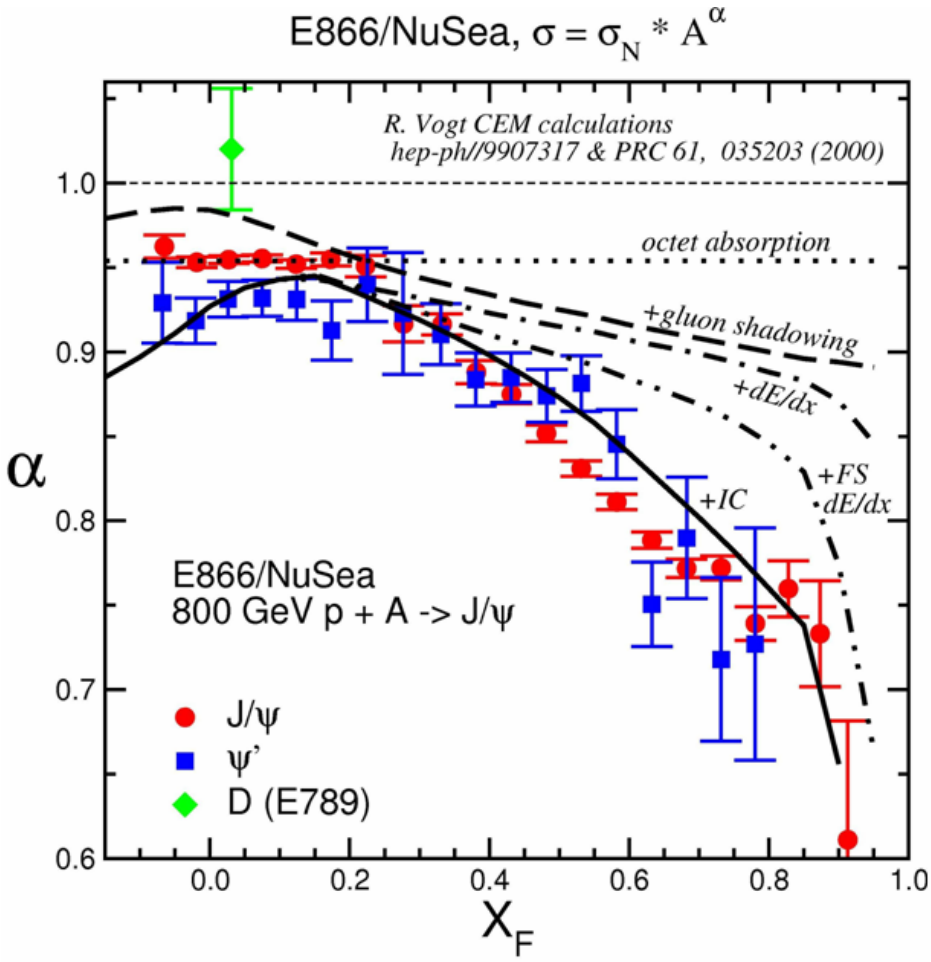

Figure 13 - J/ψ and ψ' suppression from E866/NuSea[22,23] compared to calculations from R. Vogt[24] showing the many ingredients invoked to explain the dramatic x_F dependence of the observed suppression.

These measurements of J/ψ suppression have now been extended to RHIC energies by PHENIX[25], as shown in Figure 14 compared to model calculations from R. Vogt[26] using the EKS[2] shadowing prescription and different absorption cross sections for the final-state $c\bar{c}$. Clearly, with the statistics available so far, this data is not able to constrain the absorption cross sections very well. The importance of such constraints from d+Au collisions in establishing a baseline in A+A collisions, where we look for effects beyond the cold nuclear matter (CNM) effects seen in d+Au collisions from the QGP, can be seen in Figure 15. Without a more accurate baseline from d+Au collisions one cannot conclude that the A+A collisions show suppression beyond that from CNM except at the highest centralities. A higher luminosity d+Au (or p+Au) run will be necessary in the near future in order to allow a clearer analysis of the A+A results, as well as to pin down the physics of the fundamental processes (e.g. gluon shadowing, intitial-state gluon energy loss, final-state $c\bar{c}$ absorption) that cause these CNM effects.

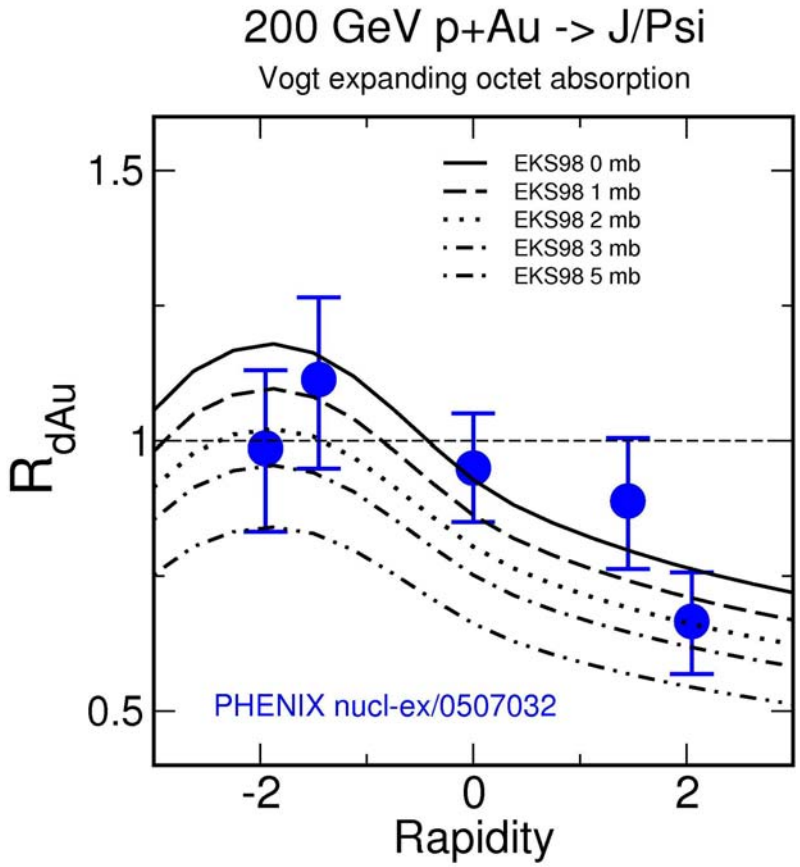

Figure 14 - J/ψ suppression at √S=200 GeV from PHENIX[25] vs rapdity compared to model calculations from R. Vogt[26] for EKS[2] shadowing and different $c\bar{c}$ absorption cross sections in the final state.

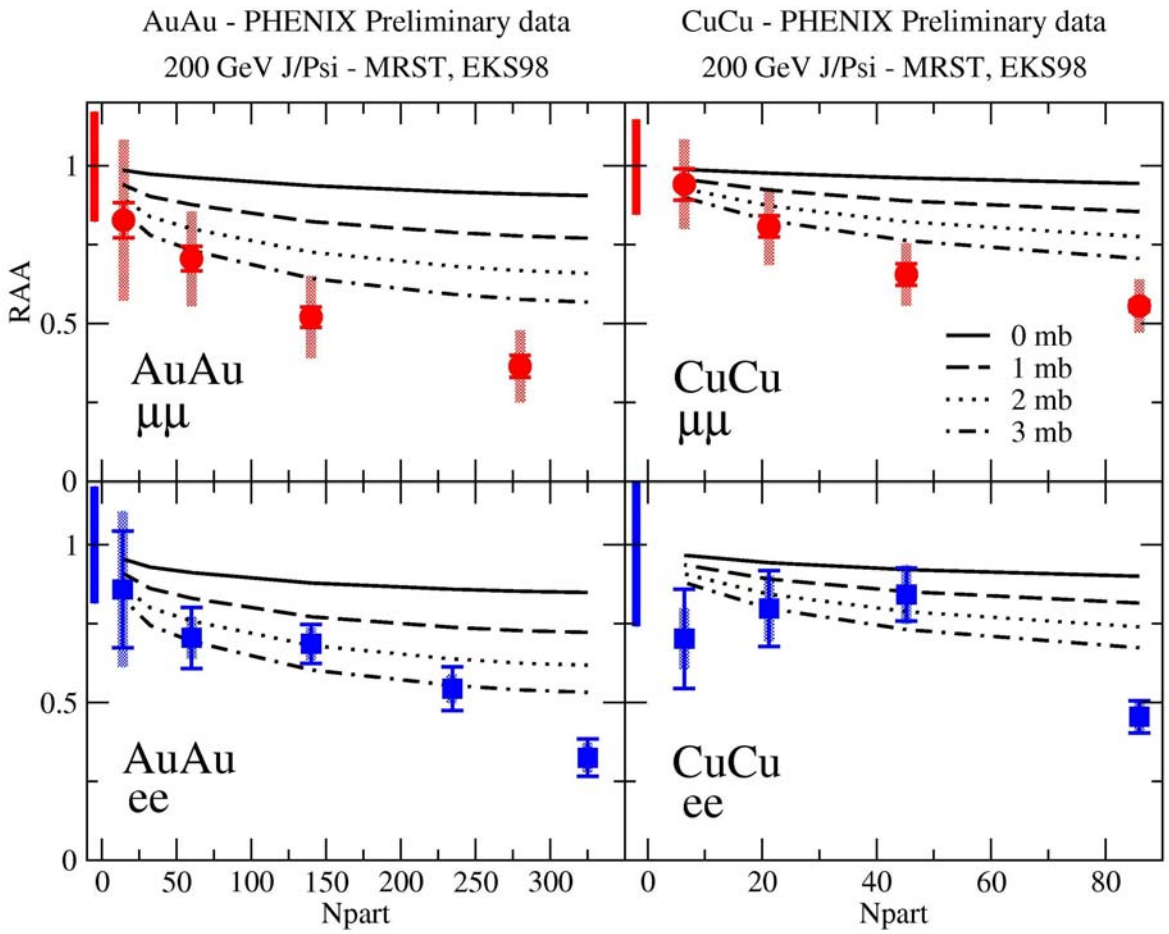

Figure 15 – Preliminary results for the nuclear modification factor in AuAu and CuCu collisions from PHENIX[27] vs centrality for forward and central rapidity compared to CNM calculations consistent with those shown in the previous figure (Figure 14).

Another outstanding part of the physics puzzle for J/ψ production in p(d)+A collisions follows from the fact that the suppression pattern does not scale with x_2 as one would expect if the dominant physics effect was nuclear shadowing or saturation. As shown in Figure 16 the nuclear suppression from PHENIX[25] at 200 GeV, E866/NuSea[22] at 39 GeV and NA3[28] at 19 GeV is not universal in x_2 but, at least for the lower energy results that span a large range in x_F, show an approximate scaling in x_F. This suggests that the dominant physics behind the suppression pattern is not shadowing or gluon saturation. As mentioned before, one interpretation from Kopeliovich et al.[7] is that instead the universal suppression at large x_F may be caused by Sudakov suppression. Roughly speaking, this picture says that one must exclude more inelastic processes as one approaches the kinematic limit (x_F = 1) and that since these potential inelastic processes become more

copious in a nucleus this effect is stronger in a nucleus and causes the observed increasing suppression as one approaches $x_F = 1$.

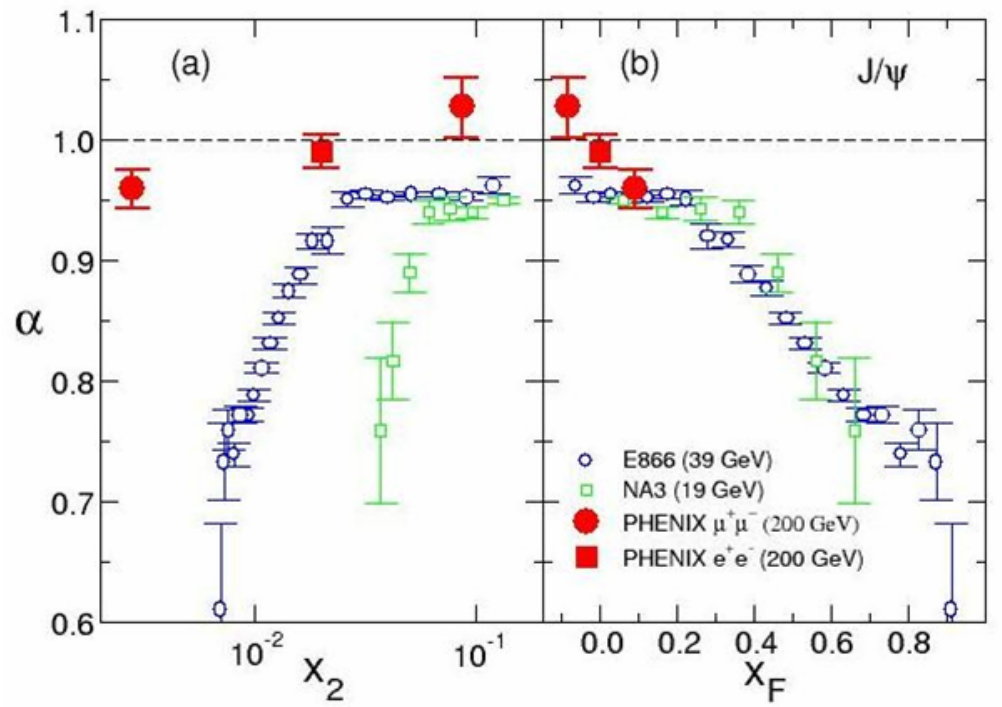

Figure 16 - Comparision of J/ψ nuclear suppression for three different beam energies showing the lack of scaling vs x_2 and approximate scaling seen vs x_F.

It is also interesting to note that the trends vs rapidity seen in J/ψ suppression are similar to those seen for light hadrons, as shown in Figure 17. This suggests a common underlying physics effect such as the Sudakov suppression mentioned above, or the phenomena discussed in the interpretation of PHOBOS data called "limiting fragmentation"[5].

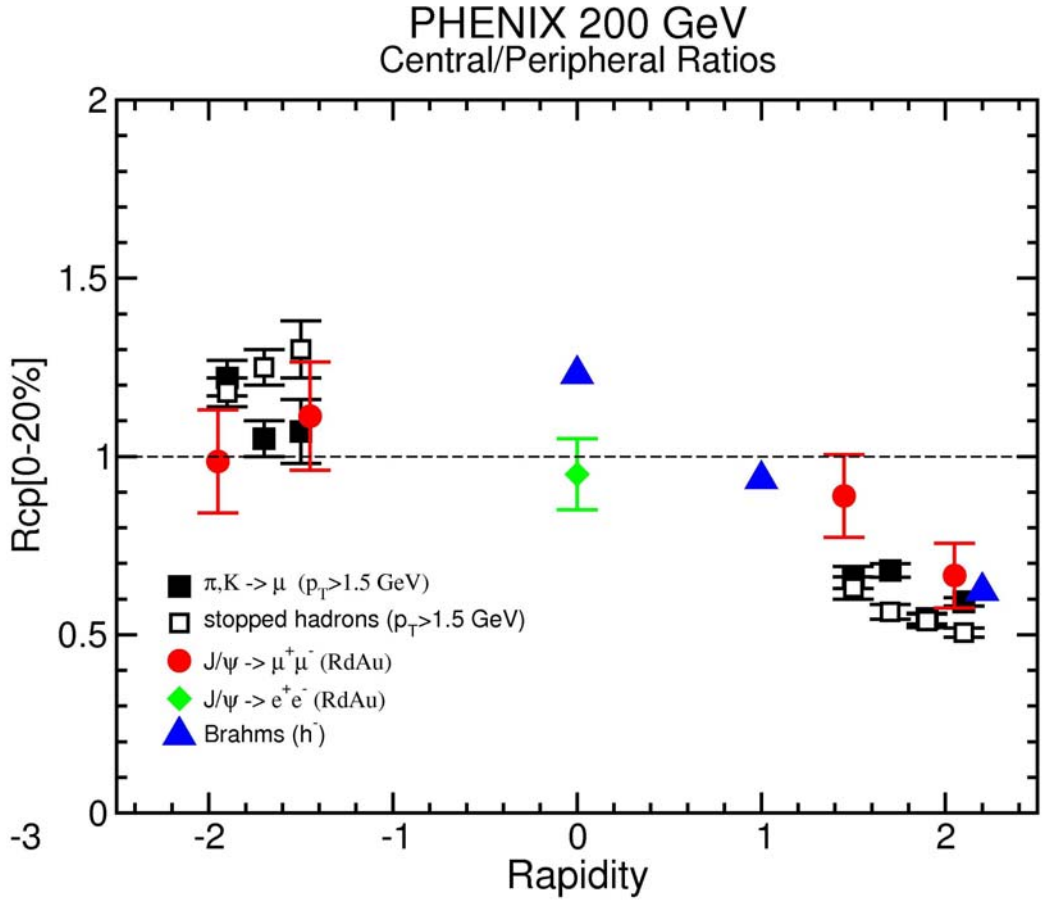

Figure 17 - Ratio of central to peripheral yields per binary collision for d+Au collisions comparison between J/ψ's (PHENIX) and light hadrons from Brahms and PHENIX. A similar pattern is seen with a small enhancement at negative rapidity (Au direction) and suppression at postitive rapidity (d direction and small-x shadowing region).

Finally, in Figure 18, we show preliminary results for ϒ production from PHENIX in the forward and backward rapidity regions[29]. These measurements are severely limited by the small cross section for ϒ's and clearly need the higher luminosity of RHIC-II to both improve the statistics of the signal and to allow better determination of the background including that from Drell-Yan pairs.

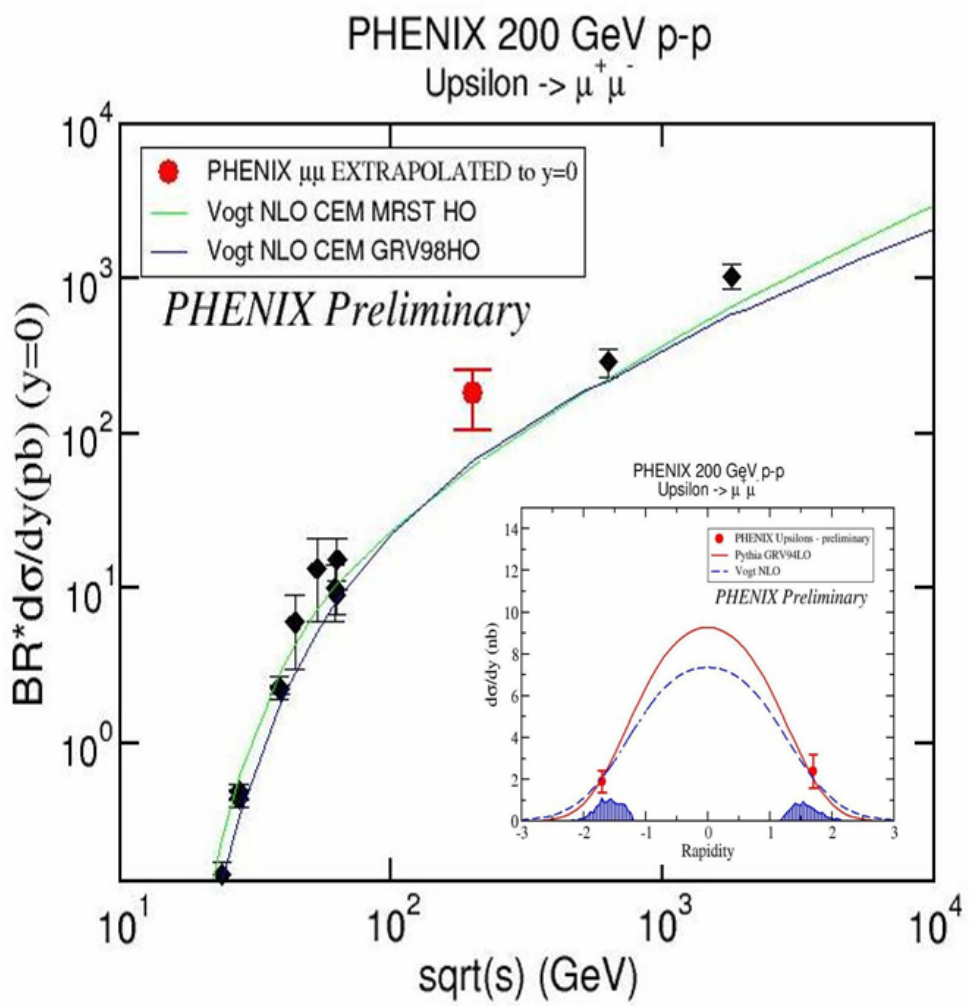

Figure 18 - Preliminary PHENIX ϒ results[29] at forward and backward rapidity (red) from 200 GeV p+p collisions compared to measurements at other energies vs energy.

5 Forward Tagged Processes

5.1 Tagged Drell-Yan Processes

An interesting possibility at RHIC-II is the study of the tagged Drell-Yan process in which Drell-Yan di-leptons are accompanied by an energetic neutron or proton carrying a large fraction of the incident proton beam momentum. Such a process is the hadronic analog of the diffractive DIS process observed recently at HERA[30]. In the HERA experiment, the DIS was tagged by a forward-going neutron or proton. These tagged DIS events can be interpreted as virtual photons scattering off the pion cloud (or pomeron) of the proton beam. The pion stricture function can be extracted from such measurements.

It is natural to extend the HERA measurement to other hard-processes tagged by forward-going nucleons. Of particular interest is the tagged Drell-Yan, which could provide new insight on the origin of the flavor asymmetry of the nucleon sea. The large $\bar{d}/\bar{u}$ asymmetry observed in Drell-Yan measurements[31] was attributed to the presence of meson cloud in the nucleon. A tagged Drell-Yan measurement would allow a direct determination of the meson cloud. A simulation for the $p + p \rightarrow \mu^+\mu^- X$ for the PHENIX detector, where the muon pairs are detected in the muon arms and the neutrons are detected by a small-angle calorimeter (such as the Zero Degree Calorimeter), has been carried out and the result is shown in Figure 19.

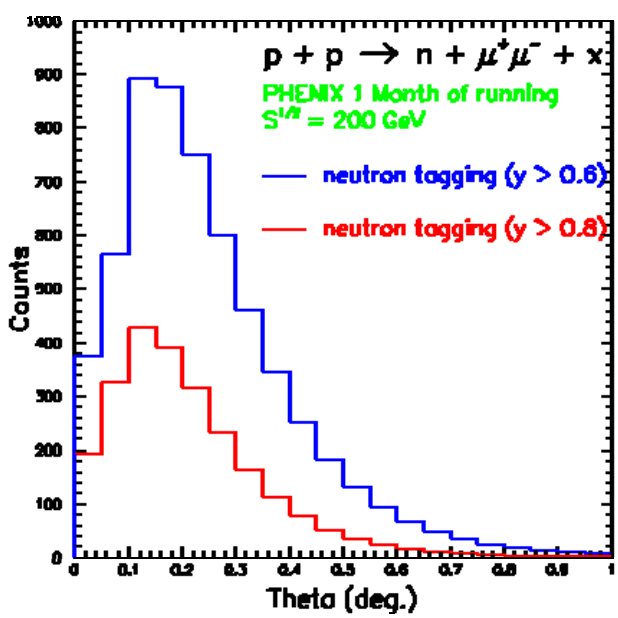

Figure 19 – Simulation of the neutron-tagged Drell-Yan process where the muons are detected in the PHENIX muon arms and the neutron in a small-angle calorimetet (e.g. the PHENIX ZDC).

The forward tagging capability could lead to many other measurements not feasible in the fixed-target experiments. For example, one could consider tagging the forward-going Δ or λ. The λ-tagging is of special interest since it can shed light on the strange-quark contents of the proton. Another possibility is the measurement of the double-helicity asymmetry, A_{LL}, in tagged the $\vec{p}\vec{p}$ Drell-Yan process. Since the underlying process involves the proton-pion interaction, A_{LL} is expected to be zero. The doubly-tagged Drell-Yan process, which involves the pion-pion interaction, can also be contemplated. Finally, it is natural to extend tagged Drell-Yan measurement to tagged J/ψ production.

5.2 Tagged Forward Protons

Wlodek Guryn?

6 Anti-quark distribution in nuclei at small x

In the past decade, quark shadowing at small x has been very well characterized experimentally in DIS[32]. The experimental signature is that the DIS cross section ratio falls below unity for $x \leq 0.08$. Theoretically, shadowing has been studied extensively in the past 10 years[33].

Quark shadowing is also expected in hadronic processes. To date, the only experimental evidence for shadowing in hadronic reactions is the reduction in the nuclear dependence seen in the Drell-Yan experiments E772[34] and E866[35]. The lowest x covered in these experiments is $x = 0.04$, just below the onset of shadowing effect.

Shadowing in the $p+A$ Drell-Yan process is largely due to antiquarks in the nucleus, unlike in DIS where both quarks and antiquarks can contribute. Although shadowing effects are expected for antiquarks, there is no known requirement that they be identical[36] to those for quarks. There exists no experimental information on the antiquark shadowing at small x ($x < 0.04$). The coverage in x_2 will be significantly extended at RHIC. In particular, the lowest x_2 reachable at RHIC is around 10^{-3}, a factor of 40 lower than in E772. Therefore, nuclear shadowing effect of antiquarks can be well studied at PHENIX using the muon arms and possibly the Nose Cone Calorimeter (NCC) which could detect Drell-Yan events via the $\mu^+\mu^-$ and e^+e^- channels, respectively.

An important role of the NCC and the forward silicon vertex detectors in the Drell-Yan measurement is that it will allow a realistic determination of the contribution of open-charm

background to the dimuon (or di-electron) events. The eμ pair events from the NCC and muon arm would lead to a direct measurement of the charm background. This would enable a reliable Drell-Yan measurement down to the smallest possible *x* values.

7 Ultra-peripheral Processes

In addition to studies of strong interactions of dense matter, RHIC also has an electromagnetic interaction program focusing on ultraperipheral collisions (UPCs) with large impact parameters, $b>2R_A$ in symmetric A+A collisions. It is possible to study electromagnetic interactions through photoproduction (a photon from one nucleus interacts with a quark or gluon from the opposite nucleus) and two-photon processes (two photons, one from the field of each nucleus) using UPCs because highly accelerated ions are surrounded by photon fields. These photons are almost real since their virtuality is less than $(\hbar c/R_A)^2$.

The photon flux is calculated using the Weiszacker-Williams method. The flux is typically greater for large *Z* nuclei since a distance *b* away from the nucleus, the flux is

$$\frac{d^3N_\gamma}{dkd^2b}=\frac{Z^2\alpha w^2}{\pi^2kb^2}\left[K_1^2(w)+\frac{1}{\gamma_L^2}K_0^2(w)\right] \qquad \textbf{[Equation 12]}$$

where $w=kb/\gamma_L$, *k* is the photon energy, γ_L is the Lorentz boost in the center-of-mass frame of the collision and $K_0(w)$, $K_1(w)$ are modified Bessel functions. The photon flux decreases exponentially above a cutoff energy determined by the size of the nucleus. In the lab frame, the cutoff is $k_{\max}\approx\gamma_L\hbar c/R_A$. In the rest frame of the target nucleus, the cutoff is boosted to $E_{\max}=(2\gamma_L^2-1)\hbar c/R_A$. Table 2 shows the beam energies, E_{beam}, Lorentz factors, γ_L, $k_{\max}$, and $E_{\max}$, as well as the corresponding maximum center of mass energy, $\sqrt{S_{\max}}=\sqrt{2E_{\max}m_p}$, for single photon interactions with protons.

Table 2 - Beam energies, E_{beam}, Lorentz factors, γ_L, photon cutoff energy in the center of mass frame, $k_{\max}$, and in the nuclear rest frame, $E_{\max}$, and equivalent nucleon-nucleon center of mass energy, $\sqrt{S_{\max}}$, for *AA* collisions at RHIC.

A	E_{beam} **(GeV)**	γ_L	$k_{\max}$ **(GeV)**	$E_{\max}$ **(TeV)**	$\sqrt{S_{\max}}$ **(GeV)**
O	125	133	8.7	2.31	66
Si	125	133	7.2	1.92	60

I	104	111	3.6	0.81	39
Au	100	106	3.0	0.66	35

The total photon flux striking the target nucleus is the integral of [Equation 12 over the transverse area of the target for all impact parameters subject to the constraint that the two nuclei do not interact hadronically. A reasonable analytic approximation for *A*+*A* collisions is given by the photon flux integrated over distances $b>2R_A$. The analytic photon flux is

$$\frac{dN_\gamma}{dk} = \frac{2Z^2\alpha}{\pi k}\left[w_R^{AA} K_0(w_R^{AA}) K_1(w_R^{AA}) - \frac{(w_R^{AA})^2}{2}\left(K_1^2(w_R^{AA}) - K_0^2(w_R^{AA})\right)\right] \qquad \textbf{[Equation 13]}$$

where $w_R^{AA} = 2kR_A/\gamma_L$.

Calculations of interactions such as heavy quark production by photon-gluon fusion, $\gamma + g \rightarrow Q\overline{Q}$, can be treated similarly to parton-parton interactions in the initial nucleon-nucleon interactions in central collisions since *k* is a continuum up to $E_{\text{beam}} = \gamma_L m_p$. Predictions for charm production in UPCs at RHIC can be found in Ref. 37. Since the photoproduction cross section is proportional to a single power of the nuclear gluon distribution, UPCs are an alternative method of measuring the gluon distributions albeit at higher *x* than in central collisions.

Presently the UPC photoproduction data at RHIC are from ρ and J/ψ measurements at STAR[38] and PHENIX[39] respectively. These vector mesons are typically produced when a photon in the field surrounding the nucleus fluctuates into $q\overline{q}$ pairs with the same quantum numbers as the photon and then materialize through elastic scattering with the nucleus, known as vector meson dominance. Since vector mesons are produced coherently by this mechanism at rather low p_T, $p_T = \hbar c/R_A \approx 100$ MeV, such measurements are better done at RHIC than at LHC. The STAR ρ event samples in *AA* collisions are large enough to study quantum interference effects. (The ρ production cross section in Au+Au collisions at STAR is about 10% of the total hadronic cross section[40].) Interference arises because either nucleus can emit the photon, so that the processes are indistinguishable[41].

Photoproduction events are relatively clean since they are typically low multiplicity. Only one nucleus breaks up, leaving a rapidity gap between the vector meson and the nucleus that emitted the photon. The PHENIX J/ψ measurement shown in Figure 20 was based on an electromagnetic excitation trigger (a neutron in one of the ZDCs) and detection of a single electromagnetic cluster with energy greater than 800 MeV. The observed e^+e^- pairs are at p_T < 50 MeV, indicating coherent production.

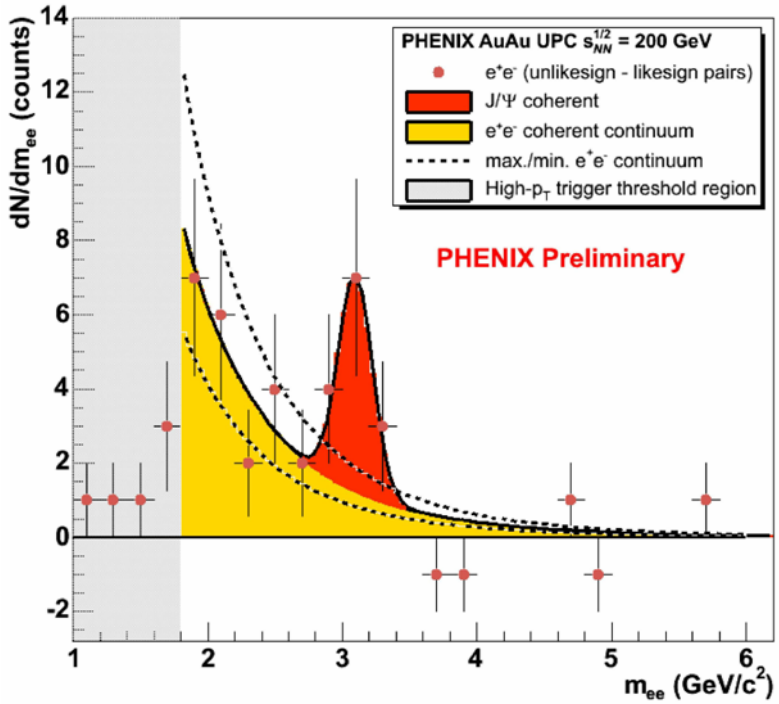

Figure 20 – J/ψs produced in ultraperipheral Au+Au collisions at RHIC from PHENIX.

8 Double Parton Correlations

Mark Strikman

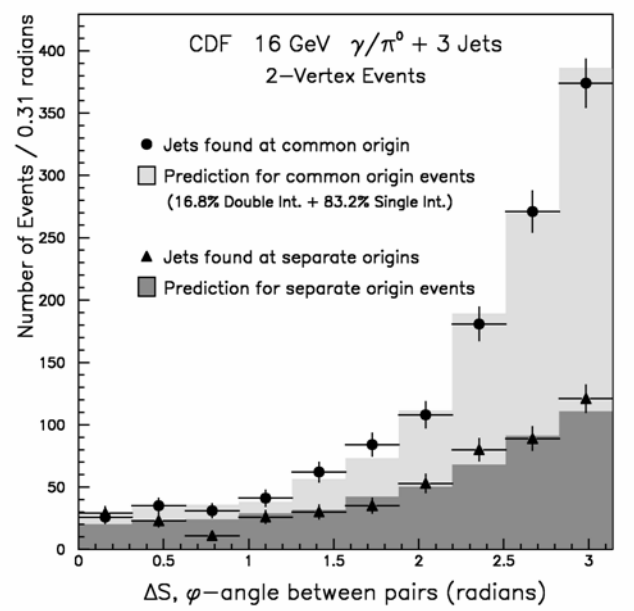

9 Comparison of RHIC-II and LHC Heavy-ion programs

10 RHIC Detector Upgrades

An active upgrade program of the major RHIC detectors is planned in order to extend their capability to more complete and robust measurements, especially in the era of RHIC-II luminosities. We will discuss each planned upgrade briefly here with an emphasis on what each brings to the forward/pA physics being discussed in this working group.

10.1 PHENIX Upgrades

10.1.1 Muon Trigger Upgrade

The PHENIX forward muon trigger upgrade is primarily intended to allow fast selection of very high momentum (p > 25 GeV/c) muons from W decays for spin measurements that will access the spin dependence of the nucleon sea. However, it will also be able to help with other triggers, in conjunction with the FVTX and NCC (see below) to allow capture of many of the more rare processes in the high-luminosity era of RHIC-II. It will also help with pattern recognition in high-occupancy events such as those from central Au-Au collisions, where present muon triggering and reconstruction is not very clean or efficient.

Resistive plate (RPC) detectors located in front of the muon arm, in between the muon tracker and muon identifier, and behind the muon identifier will be used to make a fast rough determination of the momentum which then allows rejection of lower momentum muons. The will also provide a coarse time-of-flight measurement which can be used to reject particles that do not originate at the interaction region, in particular rejecting backgrounds that come into PHENIX from the rear of the muon identifiers that are associated with the incoming beam halo. A schematic of the planned RPC arrangement (RPC's in black) is shown in Figure 21.

The project is funded by NSF; see the MRI proposal at,

https://www.phenix.bnl.gov/WWW/trigger/forwardupgrade/NSF_MRI/MRIfiles/NSF_MRI_Wboson_Final.pdf

For p(d)+A collisions, will allow level-1 triggers based on high momentum muons (p>??) that will aid in capture to tape of the more rare higher momentum events, e.g. from semi-leptonic decays of b mesons. It may also help in triggering for Υ events by requiring the higher momentum muons from these decays at the fast trigger level.

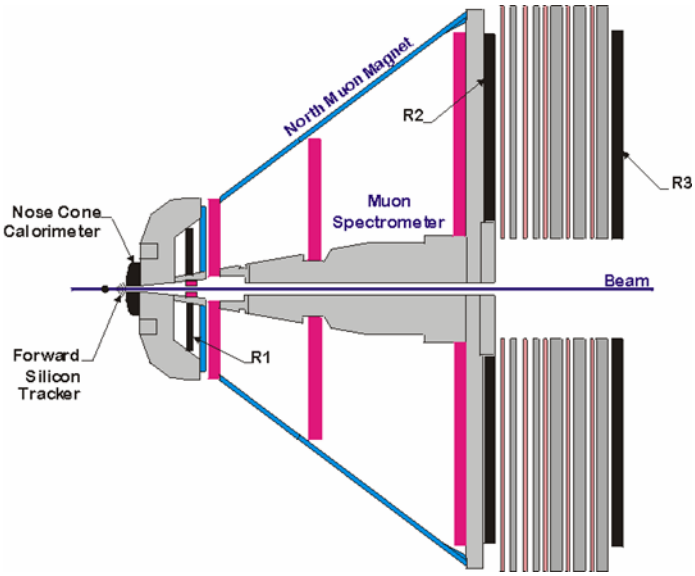

Figure 21 - PHENIX Muon Trigger upgrade (one arm shown) with its RPC planes shown in black, existing muon tracking detectors in red. The primary interaction region is at the right-center of the figure.

10.1.2 Silicon Vertex Detector

The PHENIX silicon vertex detector upgrade includes both a central rapidity barrel silicon detector (VTX) and a forward (and backward) rapidity silicon detector (FVTX). Between them they cover a rapidity range, $-2.2 < y < 2.2$, and can identify detached vertices on an event-by-event basis to isolate short and long-lived decays. This will allow the identification of open charm and beauty decays and the rejection of the longer-lived decays of light hadrons which presently contribute large backgrounds for measurements at forward and backward rapidity. The precise measurement of the tracks near the primary vertex will also improve the resolution for a number of signals including the J/ψ and Υ mass resolutions.

Figure 22 - PHENIX Silicon Vertex Detector Upgrade including the forward vertex detector (FVTX) and central barrel vertex detector (VTX).

More details than will be discussed here can be found in the CDR's for these upgrades at, http://www.phenix.bnl.gov/phenix/WWW/publish/akiba/2004/VTX_rev2/PHENIX-VTX-PROPOSAL.pdf (VTX CDR)
and
https://www.phenix.bnl.gov/phenix/WWW/publish/leitch/fvtx/ (draft FVTX CDR)

As was discussed in Section 4 with rates in Table 1, RHIC-II luminosities will be needed for many of the heavy-quark measurements since these are rare processes and rates are low for many and a large reach in p_T is important. In addition to the luminosity need, most of these measurements also need the detached vertex discrimination provided by the PHENIX silicon vertex detector upgrade. The systematics of measurements of charm and beauty via their decays to muons in forward and backward directions would remain large without the event-by-event rejection of light hadron decays which the FVTX provides. Explicit identification of beauty via the $B \rightarrow J/\psi\ X$ only becomes possible with this upgrade.

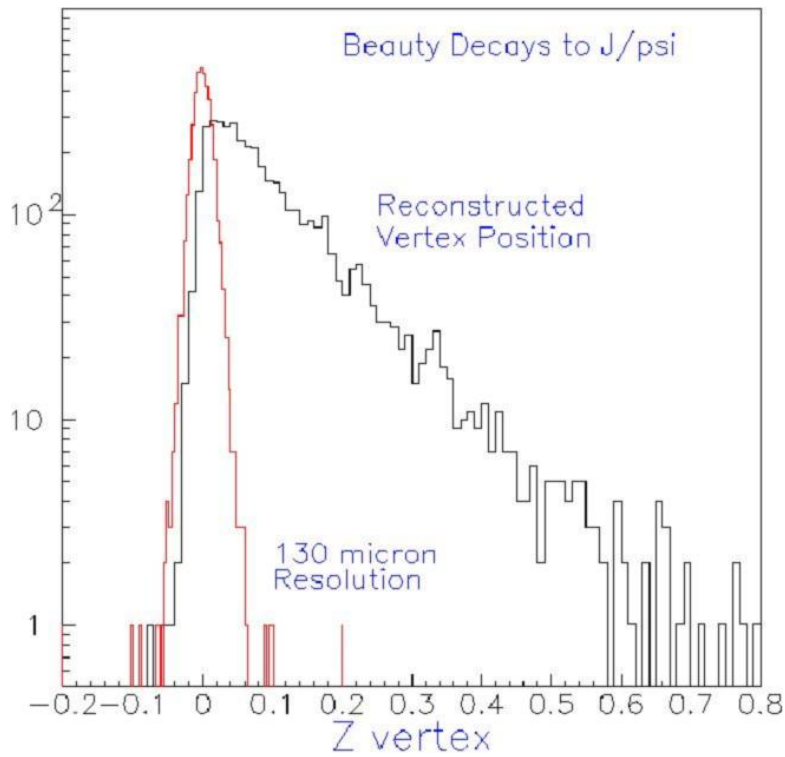

Figure 23 - The reconstructed Z-vertex distribution for J/ψ from B decays (black line) and for prompt J/ψ (red line). Note that the J/ψ yield has been scaled down by a factor of 100. The relative yield of J/ψ from B decays versus prompt J/ψ is estimated to be about 1%.

So far the mass resolution and signal-to-background in the muon spectrometers in PHENIX has not been good enough to allow a clear separation of the ψ' from the J/ψ and from the underlying background largely composed of random muon pairs from decays of light hadrons. The FVTX will both improve the mass resolution and strongly suppress the background from random pairs and will open up the study of the ψ'. The ψ' is a cleaner physics process to study since, unlike the J/ψ, it does not have a large contribution from decays of higher-mass resonances and thus all the ψ' one studies are primary.

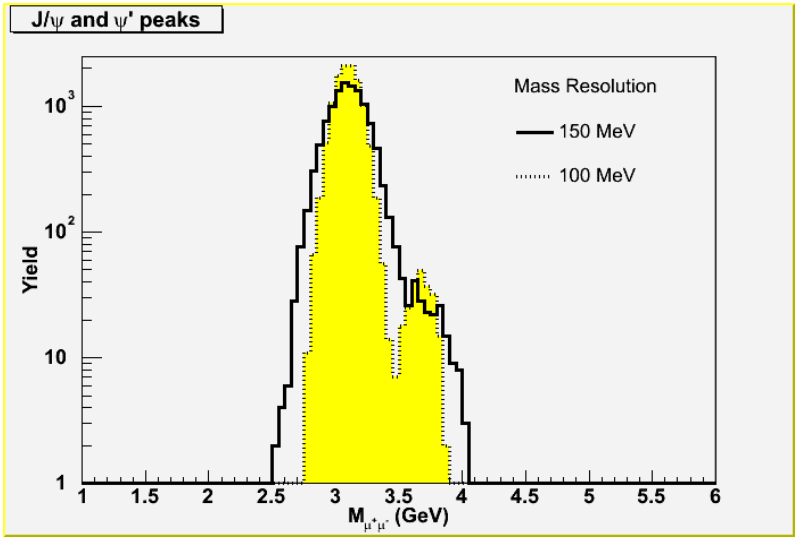

Figure 24 - Mass spectra for the J/ψ and ψ', showing the substantial improvement in separation expected with a vertex detector (yellow, 100 MeV resolution) compared to that without a vertex detector (black, 150 MeV resolution). The number of J/ψ and ψ' in this plot represents our expectation for a ~25 pb^{-1} p+p run.

10.1.3 Nose Cone Calorimeter

The PHENIX Nose Cone Calorimeter (NCC) upgrade (Figure 25) will replace the present copper nose cone hadron absorbers in the forward and backward rapidity regions in front of the muon arms with electromagnetic calorimeters. The calorimeters are tungsten layers with active silicon pads in many layers and would cover a rapidity range of $1 < |y| < 3$, providing an increase in coverage compared to the central arm calorimeters of over a factor of ten.

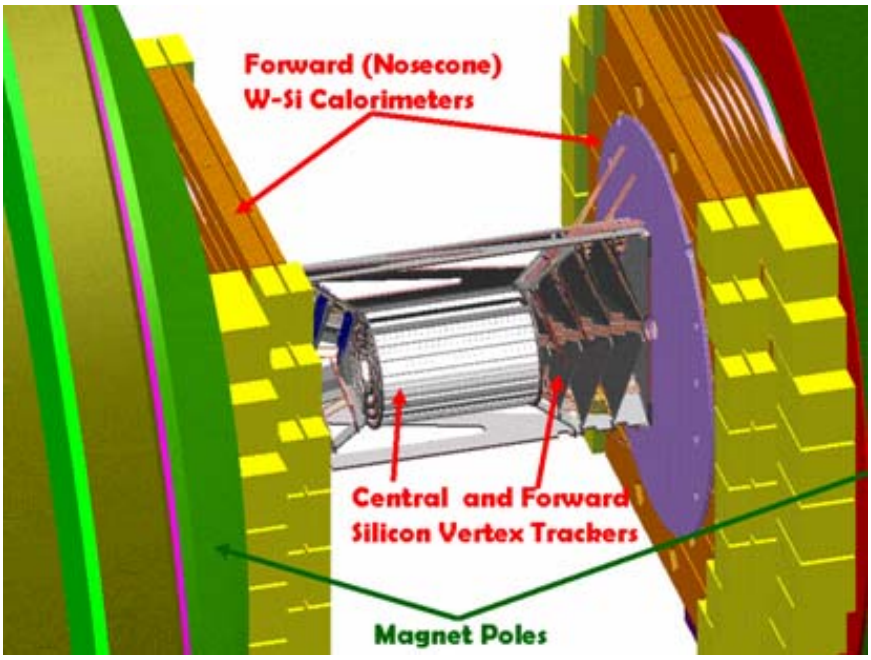

Figure 25 - PHENIX Nose Cone Calorimeter (NCC) upgrade (purple).

The NCC will add to PHENIX the capability to measure $\chi_C \rightarrow J/\psi\ \gamma$ and direct photons in the forward and backward directions. Both provide access to modifications of the gluon structure functions in these rapidity ranges which correspond to small-x of the gluon distributions where shadowing or gluon saturation effects are thought to be strong.

The χ_C is important because:

- Approximately 30% of the detected J/ψs come from its decay, and to unravel the complex puzzle of J/ψ suppression definitively will require knowing the nuclear dependence of χ_C production.
- Like the ψ', in terms of physics the χ_C is a cleaner probe of the gluons since, unlike the J/ψ, it does not suffer from feeddown from higher mass resonances.

Direct photons also provide a probe of the gluon distribution in nuclei.

A draft CDR for the NCC can be found at,

https://www.phenix.bnl.gov/WWW/publish/seto/NCC/ncccdr.pdf

10.2 STAR Upgrades

10.2.1 Forward Silicon Tracker

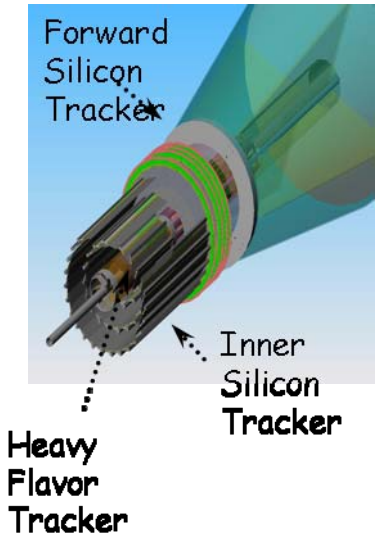

Figure 26 - STAR Forward Silicon Tracker upgrade.

10.2.2 Forward Calorimeter?

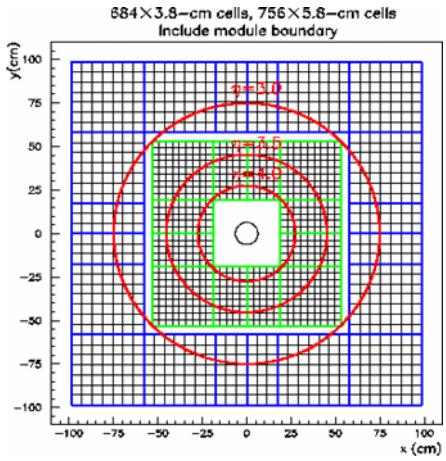

Figure 27 - STAR ? upgrade.

11 Appendix: Rates for Forward and p(d)+A Processes

	RHIC-II				LHC Heavy Ions					
Signal	PHENIX	|η|	STAR	|η|	**ALICE**	**|η|**	CMS	|η|	**ATLAS**	**|η|**
$J/\psi \to ee$	45k	<0.35	220k	<1	**9.5k**	**<0.9**				
$J/\psi \to \mu\mu$	395k	1.2-2.4			**380k**	**2.5-4**	40k	<2.4	**8-100k**	**<2.5**
$\psi' \to ee$	800	<0.35	4k	<1	**190**	**<0.9**				
$\psi' \to \mu\mu$	7.1k	1.2-2.4			**6.9k**	**2.5-4**	731	<2.4	**140-1800**	**<2.5**
$\chi_c \to ee\gamma$	2.8k	<0.35								
$\chi_c \to \mu\mu\gamma$	117k	1.2-2.4								
$\Upsilon \to ee$	400	<0.35	11.2k	<1	**1.9k**	**<0.9**				
$\Upsilon \to \mu\mu$	1.04k	1.2-2.4			**4.2k**	**2.5-4**	8.2k	<2.4	**15k**	**<2**
$B \to J/\psi \to ee$	570	<0.35	2.5k	<1						
$B \to J/\psi \to \mu\mu$	5.7k	1.2-2.4								
$D \to K\pi$	?		30k	<1	**6k**	**<0.9**				

12 Appendix: Top-down Physics Charts

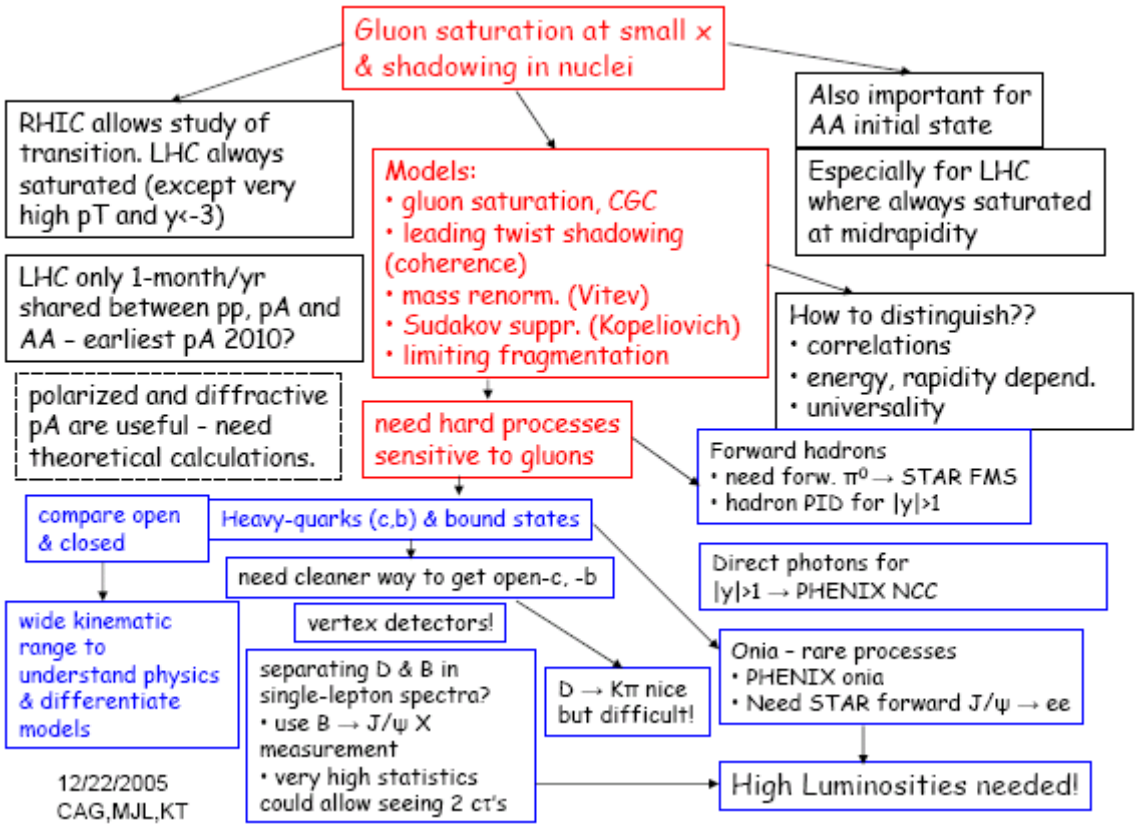

Figure 28 - Top-down physics chart for gluon saturation and shadowing in nuclei.

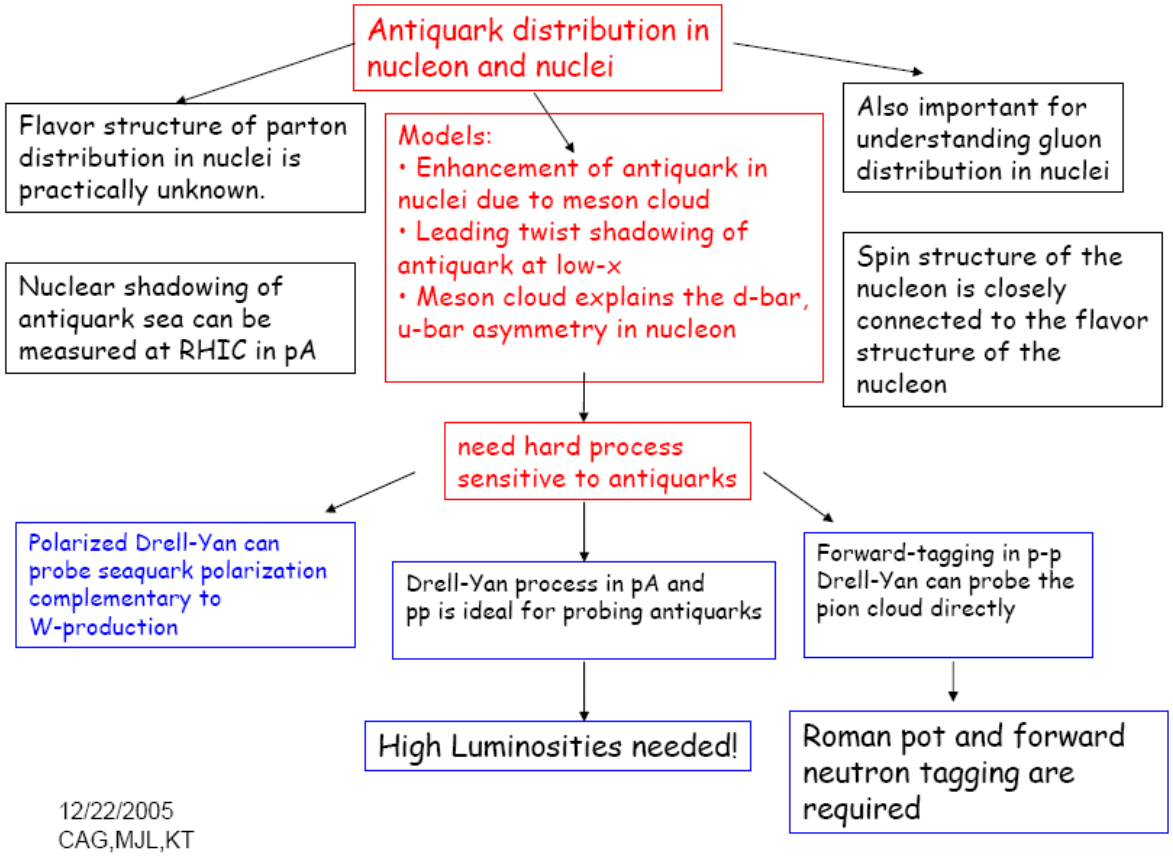

Figure 29 - Top-down physics chart for anti-quark distributions in the nucleon sea (Jen-Chieh Peng).

[1] L. McLerran and R. Venugopalan, Phys. Rev. D **49**, 2233 (1994).
[2] K.J. Eskola, V.J. Kolhinen, and C.A. Salgado, Eur. Phys. J. C **9**, 61 (1999).
[3] L. Frankfurt, V. Guzey, M. Strikman, Phys. Rev. D **71**, 054001 (2005).
[4] B. Kopeliovich, A. Tarasov, and J. Hüfner, Nucl. Phys A**696**, 669 (2001).
[5] B.B. Back et al. (PHOBOS collaboration), Phys. Rev. C **72**, 031901 (2005) and nucl-ex/0409021.
[6] I. Vitev, T. Goldman, M. Johnson and J-W Qui, hep-ph/0511220.

[7] B. Z. Kopeliovich, et al., Phys. Rev. C **72**, 054606 (2005) and hep-ph/0501260 (2005).
[8] R.C. Hwa, C.B. Yang and R.J. Fries, Phys. Rev. C **71**, 024902 (2005).
[9] D. Kharzeev, E. Levin, L. McLerran, Nucl. Phys. A**748**, 627 (200x).
[10] M. Strikman, D. Treleani, Phys. Rev. Lett. **88**, 031801 (2002).
[11] J. Nystrand, Nucl. Phys. A **752**, 470c (2005); A.J. Baltz, S.R. Klein, J. Nystrand, Phys. Rev. Lett. **89**, 012301 (2002); S.R. Klein, J. Nystrand, Phys. Rev. C **60**, 014903 (1999).
[12] J. Jalilian-Marian and Y.V. Kovchegov, Prog. Part. Nucl. Phys.**56**, 104 (2006).
[13] I. Vitev, Phys.Lett.B **562** (2003), 36.
[14] X.N. Wang Phys.Lett. B**565** (2003), 116.
[15] B.Z. Kopeliovich, J. Nemchik, I.K. Potashnikova, M.B. Johnson, I. Schmidt, Phys.Rev. **C72,** (2005)054606
[16] R. Vogt, Phys.Rev.C **70** (2004), 064902.
[17] V. Guzey, M. Strikman, W. Vogelsang, Phys.Lett. **B603**, 173 (2004).
[18] J.W.Qiu, I. Vitev, arXive:hep-ph/0405068.
[19] R.C. Hwa, C.B. Yang, R.J. Fries, Phys.Rev. **C71**(2005)024902.
[20] X.R. Wang, talk given at PANIC 05, see, http://panic05.lanl.gov/abstracts/543/
[21] J. Adams et al. (STAR collaboration), Phys. Rev. Lett. **94**, 062301 (2005).
[22] M.J. Leitch, et al., (E866/NuSea collaboration), Phys. Rev. Lett. **84**, 3256 (2000).
[23] M.J. Leitch et al., (E789 collaboration), Phys. Rev. Lett. **72**, 2542 (1994).
[24] R. Vogt, Phys. Rev. C **61**, 035203 (2000).
[25] S.S. Adler et al., (PHENIX collaboration), nucl-ex/0507032 (2005).
[26] R. Vogt, M.J. Leitch, private communication and to be published.
[27] Hugo Pereira (PHENIX) talk at QM05, see
http://qm2005.kfki.hu/Talks/Konferencia/aug6/1720//1720_hugo_pereira.ppt
[28] J. Badier, et al., (NA3), Z. Phys. C **20**, 101 (1983).
[29] M.J. Leitch, poster at QM05, see
http://www.phenix.bnl.gov/phenix/WWW/publish/leitch/posters/qm05/upsilon_poster_qm05.ppt
[30] C. Adloff et al., Eur. Phys. J. **C6** (1999) 587.
[31] E.A. Hawker et al., Phys. Rev. Lett. **80**, 3715 (1989); J.C. Peng et al, Phys. Rev. **D58**, 092004 (1998).
[32] P. Amaudruz *et al.* (NMC), Nucl. Phys. **B441**, 3 (1995).
[33] D. F. Geesaman, K. Saito, A. W. Thomas, Annu. Rev. Nucl. Part. Sci. **45**, 337 (1995).
[34] D. A. Alde *et al.* (E772), Phys. Rev. Lett. **64**, 2479 (1990).
[35] M. A. Vasiliev *et al.* (E789), Phys. Rev. Lett. **83**, 2304 (1999).
[36] L. L. Frankfurt, M. I. Strikman, S. Liuti, Phys. Rev. Lett. **65**, 1725 (1990).
[37] S. R. Klein, J. Nystrand and R. Vogt, Phys. Rev. C **66**, 044906 (2002).
[38] C. Adler *et al.* (STAR Collaboration), Phys. Rev. Lett. **89**, 272302 (2002).
[39] David D'Enterria (PHENIX collaboration), Quark Matter 2005 poster, nucl-ex/0601001, or see
http://www.phenix.bnl.gov/phenix/WWW/publish/enterria/qm05_upc_poster.
[40] G. Baur, K. Hencken, D. Trautmann, S. Sadovsky, Y. Kharlov, Phys. Rept. **364**, 359 (2002).
[41] S. Klein, arXiv:nucl-ex/0310020; arXiv:nucl-ex/0402007.